agriculture

MDPI

Article

Machine Learning Analysis of Weather-Yield Relationships in Hainan Island's Litchi

Linyi Feng [1], Chenxiao Shi [2,*], Zhiyu Lin [1], Ruijuan Li [1], Jiaquan Ning [1], Ming Shang [3], Jingying Xu [1] and Lei Bai [1,4,*]

[1] School of Ecology, Hainan University, Haikou 570228, China; fenglinyi@hainanu.edu.cn (L.F.)
[2] Hainan Meteorological Information Center, Key Laboratory of South China Sea Meteorological Disaster Prevention and Mitigation Hainan Province, Haikou 570203, China
[3] School of Earth Science and Engineering, Hebei University of Engineering, Handan 056000, China
[4] Hainan Intelligent Low-Altitude Meteorological Big Data Research Centre, Haikou 570311, China
* Correspondence: shichenxiao@hims.ac.cn (C.S.); caecar@hainanu.edu.cn (L.B.)

Abstract

Litchi (*Litchi chinensis* Sonn.) is a pillar of the tropical agricultural economy in southern China, yet its production faces increasing instability due to climate change. Traditional agronomic models often fail to capture the complex, non-linear interactions between meteorological drivers and yield formation in perennial fruit trees. To address this challenge, the study constructed a yield prediction framework using an optimized Random Forest (RF) model integrated with interpretable machine learning (SHAP), based on a comprehensive dataset from 17 major production regions in Hainan Province (2000–2022). The model demonstrated robust predictive capability at the provincial scale (R^2 = 0.564, RMSE = 2.1 t/ha) and high consistency across regions (R^2 ranging from 0.51 to 0.94). Feature importance analysis revealed that heat accumulation (specifically growing degree days above 20 °C) is the dominant driver, explaining over 85% of yield variability. Crucially, scenario simulations uncovered asymmetric climate risks across phenological stages: while moderate warming generally enhances yield by promoting vegetative growth and ripening, it acts as a stressor during the Fruit Development stage, where temperatures exceeding 26 °C trigger yield decline. Furthermore, the yield penalty for drought during Flowering (−8.09%) far outweighed the marginal benefits of surplus rainfall, identifying this window as critically sensitive to water deficits. These findings underscore the necessity of phenology-aligned adaptation strategies—specifically, securing irrigation during flowering and deploying cooling interventions during fruit development—providing a data-driven basis for climate-smart management in tropical agriculture.

Keywords: litchi yield; climatic factors; phenological period; machine learning; crop model; tropical agriculture; growing degree days (GDD); yield prediction; climate adaptation

Check for updates

Received: 14 December 2025
Revised: 10 January 2026
Accepted: 12 January 2026
Published: 16 January 2026

Copyright: © 2026 by the authors. Licensee MDPI, Basel, Switzerland. This article is an open access article distributed under the terms and conditions of the Creative Commons Attribution (CC BY) license.

1. Introduction

Litchi (*Litchi chinensis* Sonn.) is a cornerstone of the tropical agricultural economy in southern China. As the world's largest producer, China accounts for over 70% of global cultivation, serving as a vital income source for farmers in Guangdong, Guangxi, and Hainan [1,2]. It is evident that Hainan Island occupies a distinctive strategic position, given its status as the sole tropical litchi base within the country. Its early-ripening varieties, such as 'Guizhuali' and 'Feizixiao', enter markets in early spring, commanding premium prices and balancing the national fruit supply [3]. However, the stability of this industry is

increasingly threatened by meteorological variability. The growth cycle of litchi depends critically on specific climatic conditions during distinct phenological stages, such as winter chilling for floral induction and optimal thermal time for fruit set [4,5]. The phenomenon of global climate change has intensified this vulnerability primarily through the mechanisms of rising temperatures and irregular seasonal patterns [6,7]. In Hainan specifically, extreme weather events pose severe risks; for instance, super typhoons can cause catastrophic mechanical damage to orchards in northern regions, compromising tree vigor and future production potential [8].

The primary challenge in forecasting litchi yield lies in the complex, nonlinear nature of weather–yield relationships. Meteorological drivers often impact physiological processes through strict thresholds rather than linear trends [9]. For example, while accumulated chilling is essential for floral induction [10,11], temperatures dropping below specific limits during anthesis can cause irreversible floral damage [12]. Similarly, precipitation exhibits a dual role: adequate soil moisture is critical for fruit enlargement, whereas excessive rainfall during flowering disrupts pollination and induces fungal diseases [13,14]. Moreover, these climatic effects are often synergistic; heat stress is known to be significantly exacerbated when coupled with moisture deficits [15]. Traditional agrometeorological studies have largely relied on linear regression models or simple correlation analyses [16,17]. While these methods are useful for establishing baselines, they often struggle to capture such threshold effects and complex interactions, which limits their predictive accuracy in the face of increasing climate uncertainty [18,19].

To overcome these methodological limitations, machine learning (ML) has emerged as a transformative tool in agricultural data analysis [20]. Algorithms such as Random Forest (RF), Support Vector Regression (SVR), and gradient boosting have demonstrated superior capability in modeling non-linear dependencies in high-dimensional datasets [21,22]. In recent years, ML approaches have been successfully applied to staple crops such as maize, wheat, and rice, outperforming traditional statistical models by effectively identifying critical climate drivers [23–25]. Furthermore, recent advancements in Explainable Artificial Intelligence (XAI) now allow researchers to interpret these "black box" models, thereby unveiling biological insights from data patterns [26,27]. However, the application of these advanced techniques to perennial tropical fruit trees remains underexplored [28]. Most existing litchi models are based on subtropical data and fail to account for the unique tropical monsoon climate of Hainan [29,30]. Furthermore, few studies have leveraged the interpretability of ensemble learning methods to systematically identify the critical meteorological drivers governing yield formation across distinct phenological stages (e.g., shoot growth, flowering, and fruit development) [31].

Therefore, this study aims to bridge this gap by constructing a yield prediction model for Hainan litchi. The proposed approach involves the integration of a Random Forest method with interpretable ML techniques. We integrated county-level yield records (2000–2022) with long-term daily meteorological data. The specific objectives are to (1) develop a robust ML model tailored to the tropical agro-climatic conditions of Hainan; (2) quantify the nonlinear response of yield to meteorological factors across critical phenological stages using SHAP analysis; and (3) evaluate the model's performance in capturing interannual yield variability and spatial heterogeneity. This research provides a novel, data-driven perspective for understanding tropical litchi–climate dynamics, offering scientific support for precision management and adaptation strategies.

2. Materials and Methods

2.1. Overview of the Study Area

Hainan Province (18°10′–20°10′ N, 107°50′–119°10′ E), China's sole tropical island province, covers approximately 35,400 km^2 and is characterized by a tropical monsoon climate. The topography features a central mountainous core (Wuzhishan Mountains) surrounded by coastal plains (Figure 1). Mean annual temperatures range from 22.4 to 27.5 °C, with effective accumulated thermal units (≥10 °C) reaching 8500–9300 °C·d annually. Annual precipitation averages 1600 mm, with a pronounced wet season (May–October) accounting for over 80% of the total, complemented by 2000–2600 h of sunshine. These conditions establish high suitability for litchi cultivation. However, the region faces two primary climatic constraints: frequent typhoon disturbances (mean 3.7 landfalls annually) and severe dry-season drought in western areas (precipitation < 300 mm). Long-term meteorological data (2000–2022) confirm a consistent warming trend (Appendix B.1, Figure A4).

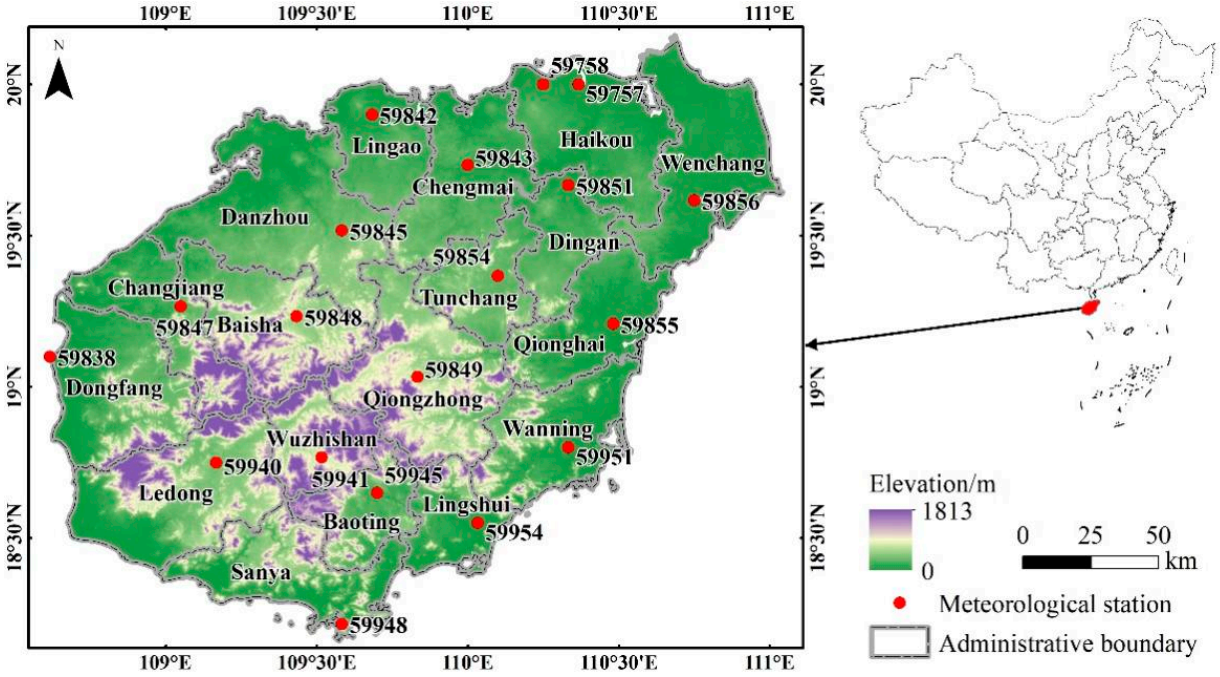


Figure 1. Meteorological Stations in Hainan Province with Topographic Features. The numbers on the map correspond to the meteorological stations and their World Meteorological Organization (WMO) codes: Haikou (59758, 59757), Wenchang (59856), Qionghai (59855), Wanning (59951), Lingshui (59954), Baoting (59945), Sanya (59948), Ledong (59940), Wuzhishan (59841), Ding'an (59851), Tunchang (59854), Chengmai (59843), Lingao (59842), Danzhou (59845), Changjiang (59847), Dongfang (59838), Baisha (59848), and Qiongzhong (59849). Hainan's litchi industry underwent a structural transformation from 2000 to 2022, shifting from area-driven to productivity-driven growth (Figure 2). During 2000–2007, total output expansion relied primarily on cultivation area increase (from 5000 to 19,500 ha, annual growth rate 21.5%). From 2008 onward, planting area stabilized (~18,500–20,000 ha), and output growth became dependent on yield improvements (2.15% year^{-1}). Despite this intensification—total production rising from 42,000 to 218,000 tons—significant interannual yield volatility persisted (coefficient of variation 15.3%), underscoring ongoing vulnerability to climate variability.

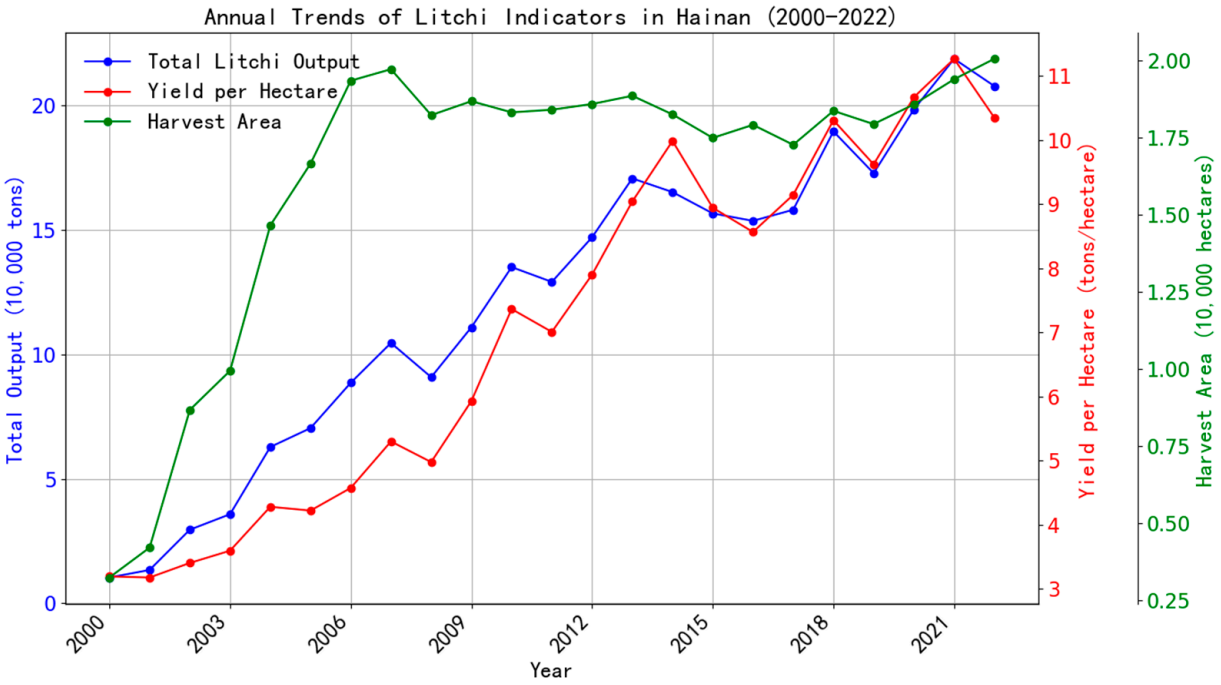


Figure 2. Temporal trends in litchi production indicators: total yield, yield per ha, and harvested area in Hainan Province (2000–2022).

2.2. Data Acquisition and Preprocessing

This study utilizes annual litchi production data (2000–2022) from 17 major growing regions in Hainan Province, sourced from the "Hainan Statistical Yearbook" (2001–2023) [32]. A small portion of missing annual yield values (2.3%) was imputed using the k-nearest neighbors (k = 5) algorithm, a widely adopted method in agricultural yield prediction studies for handling random missing data [33]. For each missing record, the five most similar complete feature vectors (based on regional meteorological characteristics) were identified using Euclidean distance, and the missing yield was imputed by the mean of the corresponding yields from these neighbors. The k = 5 parameter was selected through sensitivity analysis to balance bias and variance. Little's MCAR test confirmed the missing pattern was random (p = 0.147), supporting the suitability of k-NN, which performs reliably under low missing rates [34]. Corresponding daily meteorological data were obtained from the China Meteorological Data Network, including maximum/minimum/mean temperature (T_max, T_min, T_avg), precipitation (P), and solar radiation (R_s). Based on established phenological characteristics, the annual growing season was divided into five distinct stages (Table 1). For each stage, we constructed a comprehensive set of meteorological features: (1) aggregated metrics (mean, maximum, minimum values of temperature, precipitation, and radiation); (2) GDD calculated using physiological thresholds of 5 °C, 10 °C, 15 °C, and 20 °C to capture thermal requirements; (3) temporal trend coefficients computed via 30-day sliding windows; and (4) interaction terms between meteorological variables and phenological stages to capture stage-specific climate sensitivities. Data quality control included outlier detection using the interquartile range rule, missing value imputation via k-nearest neighbors (k = 5), and spatial consistency checks. All numerical features were standardized, and phenological stages were encoded as ordinal labels (ASG = 1, FBD = 2, FL = 3, FD = 4, MAT = 5) to preserve temporal sequencing.

Table 1. Phenological stage divisions for litchi in Hainan Province.

Stage Name	Period	Key Physiological Process
Autumn Shoot Growth (ASG)	1 August–31 October	Vegetative growth, nutrient accumulation
Flower Bud Differentiation (FBD)	1 November–31 January	Floral induction under chilling
Flowering (FL)	1 February–15 March	Anthesis, pollination
Fruit Development (FD)	16 March–15 May	Cell division and enlargement
Maturation (MAT)	16 May–31 July	Sugar accumulation, ripening

2.3. Machine Learning Models

A suite of machine learning algorithms was developed and compared to identify the optimal approach for litchi yield prediction. Candidate models include: Multiple Linear Regression (MLR) as a statistical baseline; Lasso and Ridge regression for addressing multicollinearity; ensemble tree-based methods capable of capturing nonlinear relationships (Random Forest, Gradient Boosting Decision Trees, Extreme Random Trees); Support Vector Regression (SVR) for high-dimensional feature spaces; and Artificial Neural Networks (ANN) for deep feature learning.

Two validation strategies were employed to ensure model robustness and generalizability. First, random split validation partitioned the entire dataset into training (80%) and testing (20%) using a fixed random seed of 42. This approach ensured reproducibility and a balanced representation of spatial, phenological, and meteorological variability across both sets. The final model performance metrics reported in the Results section, including R^2, RMSE, and MAE, are derived exclusively from predictions on this held-out test set, thereby demonstrating its predictive capability on unseen data. Second, temporal validation assessed the model's ability to capture interannual trends by training on 80% of chronologically earlier data and testing on the remaining 20%.

Model training incorporated 5-fold cross-validation with Bayesian optimization to tune key hyperparameters (e.g., tree depth, number of estimators, regularization coefficients). The best-performing model was further refined using Randomized Search CV to determine the optimal configuration. Performance was evaluated using root mean square error (RMSE), mean absolute error (MAE), and coefficient of determination (R^2).

To enhance interpretability, the SHAP (Shapley Additive Explanations) framework was applied to the optimal model to quantify the marginal contribution and directional impact of each meteorological driver on yield predictions across different phenological stages.

All data analysis and machine learning modeling were performed within a Jupyter Notebook environment using Python 3 (v3.9.13). Key Python libraries employed include: scikit-learn (v1.6.1) for model construction and the k-nearest neighbors imputation; SHAP (v0.48.0) for interpretability analysis; pandas (v2.2.3) and NumPy (v1.24.4) for data manipulation; and Matplotlib (v3.5.2) and Seaborn (v0.13.2) for visualization.

2.4. Climate Scenario Simulation

To quantify litchi yield responses to potential climate extremes, a series of perturbation scenarios was constructed by systematically adjusting historical meteorological records. Baseline climate variables were modified as follows: temperature (T) by ± 2 °C, GDD by $\pm 10\%$, precipitation (P) by ± 30 mm, and solar radiation (R_s) by ± 60 W·m^{-2}. An additional extreme scenario applied $\pm 30\%$ perturbations to all factors simultaneously to evaluate compound climate stress. Given that provincial-scale yield dynamics are better represented at annual resolution, the optimized Random Forest model was retrained using year-aggregated meteorological predictors. This annually calibrated model was then applied to each perturbed scenario to generate corresponding yield projections. Sensitivity coefficients were calculated as the percentage change in predicted yield per

10% change in each climatic driver, enabling standardized comparison across factors and phenological stages.

3. Results

3.1. Construction and Performance Evaluation of the Yield Prediction Model

3.1.1. Model Selection and Overall Performance

A comparative evaluation of machine learning algorithms identified Random Forest (RF) as the optimal approach for litchi yield prediction (Table 2). RF achieved the highest test set accuracy (R^2 = 0.515, RMSE = 2.237 t/ha, MAE = 1.477 t/ha), followed by Gradient Boosting Decision Trees (GBDT, R^2 = 0.488). In contrast, linear models (Multiple Linear Regression, Lasso, Ridge) and other nonlinear methods (Support Vector Regression, Artificial Neural Networks) exhibited substantially lower performance, with R^2 values ranging from 0.083 to 0.293. This performance gap demonstrates the advantage of tree-based ensemble methods in capturing nonlinear climate-yield relationships. RF was ultimately selected based on three main considerations: (1) Performance: RF achieved the highest predictive accuracy among all tested models (R^2 = 0.515) (Table 2), explaining 5.51% more variance than the second-best model (GBDT, R^2 = 0.488); (2) Interpretability: RF provides native feature importance measures (Gini impurity) that are highly consistent with SHAP-derived importance (Spearman's ρ = 0.816, $p < 0.01$), enabling transparent identification of key meteorological drivers—a critical requirement for generating actionable agronomic insights; (3) Robustness: RF exhibited greater stability—a well-documented advantage of its bagging mechanism over sequential boosting methods like GBDT This was evidenced by its lower performance variance across validation folds and the close agreement between its out-of-bag error and test-set error, the latter being a reliable estimator of generalization error [35,36]. Hybrid methods (e.g., RF-SVR ensembles, RF-ANN stacking) were evaluated, but the performance gain was limited (R^2 increased by 2.1%) at the cost of significantly increased complexity and reduced interpretability, and we prioritized practical implementation for agricultural stakeholders. Based on these results, RF was selected for hyperparameter optimization using Bayesian tuning with 5-fold cross-validation. The optimized model achieved improved performance (R^2 = 0.564, RMSE = 2.122 t/ha, MAE = 1.500 t/ha), confirming the effectiveness of systematic parameter search. These optimized metrics were used for all subsequent analyses.

Table 2. Performance comparison of different machine learning models for litchi yield prediction.

Model	RMSE (t/ha)	MAE (t/ha)	R^2
Multiple Linear Regression	2.704	2.054	0.291
Lasso Regression	3.076	2.542	0.083
Ridge Regression	2.701	2.053	0.293
Random Forest	2.237	1.477	0.515
Gradient Boosting Decision Tree	2.299	1.651	0.488
Support Vector Regression	2.785	2.069	0.248
Artificial Neural Network	2.804	2.089	0.238
Extra Trees	2.694	1.865	0.297

3.1.2. Regional Model Performance

Temporal validation of predicted versus observed yields (2000–2022) demonstrated robust model performance across regions (Figure 3). Predicted trajectories closely tracked long-term trends and interannual variability, with R^2 ranging from 0.85 to 0.95, RMSE between 0.61 and 1.26 t/ha, and MAE between 0.46 and 1.07 t/ha. Year-by-year analysis reveals that major prediction deviations often align with documented extreme events. Model accuracy

varied spatially. Wanning achieved the highest performance (R^2 = 0.95, RMSE = 0.62 t/ha), followed by Lingshui and Haikou (R^2 = 0.94, RMSE = 0.61–0.64 t/ha). For instance, the underprediction in Haikou around 2014 corresponds to the severe impact of Super Typhoon Rammasun. Lingao and Wenchang showed moderate fit (R^2 = 0.87–0.91), with slightly elevated MAE (0.65–0.83 t/ha) indicating larger deviations during extreme yield years. Ding'an exhibited the weakest performance (R^2 = 0.85, RMSE = 1.26 t/ha), with systematic bias—underestimating peak yields while overestimating low yields. The model notably failed to capture the low yield around 2016–2017, likely related to compounded stresses from Typhoon Dianmu. This pattern suggests reduced model capacity in heterogeneous environments, likely due to complex topography or unaccounted management practices. Furthermore, observed yield declines in years such as 2003 and 2020 align with non-climatic disruptions (SARS and COVID-19 control measures), which are not represented in the climate-driven model. Despite regional variation, the model demonstrates operational utility for yield forecasting across major production zones.

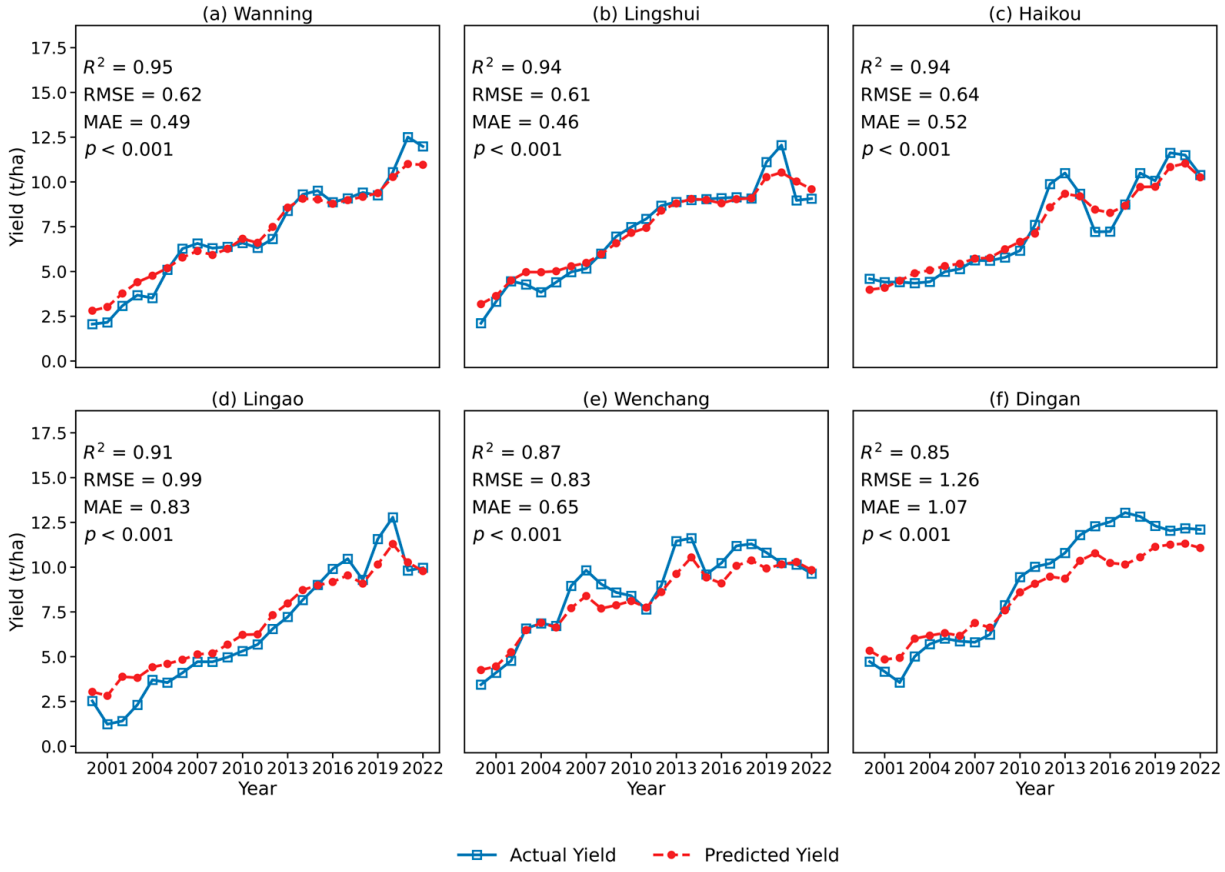


Figure 3. Temporal analysis of observed vs. predicted litchi yields in selected regions of Hainan Province (2001–2022). The plots compare actual yield (blue dashed line) with model-predicted yield (red solid line), The model demonstrated high fit in these six regions ($R^2 \geq 0.85$), effectively capturing long-term yield trends But predictive precision for interannual fluctuations varied across regions, as further detailed plots for the remaining 11 regions are provided in Appendix D.4.

Spatial distribution of out-of-fold prediction errors revealed distinct regional bias patterns (Figure 4). The northeastern coastal plain (Wenchang, Qionghai, Ding'an) showed systematic overestimation (+0.43 to +0.51 t/ha), while the central mountainous zone exhibited underestimation, particularly in Baoting (−0.51 t/ha), Tunchang (−0.32 t/ha), and Qiongzhong (−0.18 t/ha). Baisha (+0.42 t/ha) was an exception within this region. The western areas displayed heterogeneous errors, with severe underestimation in Chengmai (−0.60 t/ha), Lingao (−0.41 t/ha), and Changjiang (−0.41 t/ha), contrasting with moder-

ate overestimation in Danzhou (+0.36 t/ha). The most accurate predictions occurred in southeastern coastal counties (Wanning, Haikou, Lingshui) and southern areas (Sanya), where absolute errors remained below ±0.10 t/ha. Overall, prediction accuracy declined in topographically complex central-western regions, indicating potential benefits from incorporating terrain and soil covariates.

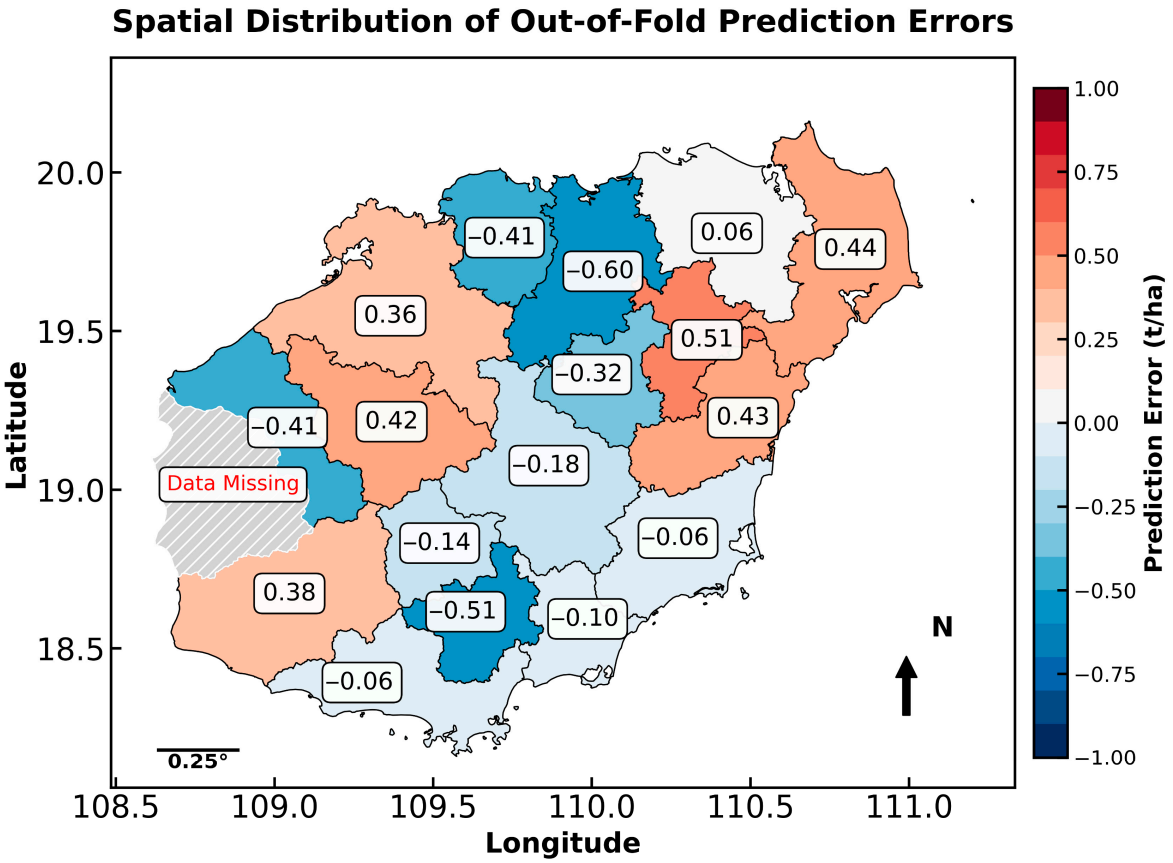


Figure 4. Spatial distribution of out-of-fold prediction errors (OOF) prediction error (Predicted Yield − Actual Yield, in t/ha) for litchi yield across Hainan Province. Positive values (red shades) indicate an overestimation of litchi yield, while negative values (blue shades) indicate an underestimation.

3.2. Identification and Contribution Analysis of Key Meteorological Drivers

3.2.1. Ranking of Feature Importance

SHAP analysis identified heat accumulation as the dominant yield driver (Figure 5). GDD_20 exhibited the highest importance (0.338), with predominantly positive SHAP values indicating a consistent yield-enhancing effect. Mean temperature ranked second (0.221), also showing positive associations. In contrast, precipitation and radiation displayed dispersed, bidirectional SHAP distributions, reflecting variable and context-dependent effects. Collectively, the four GDD indices accounted for 85.3% of total feature importance (cumulative contribution: 0.853), far exceeding precipitation (0.125) and radiation (0.117). This ranking, derived from the Random Forest model's Gini impurity metric, is visually summarized in Figure A8. This hierarchy remained consistent across evaluation methods, with strong correlation between Gini-based importance and mean |SHAP| values (Spearman's $\rho = 0.816$, $p < 0.01$).

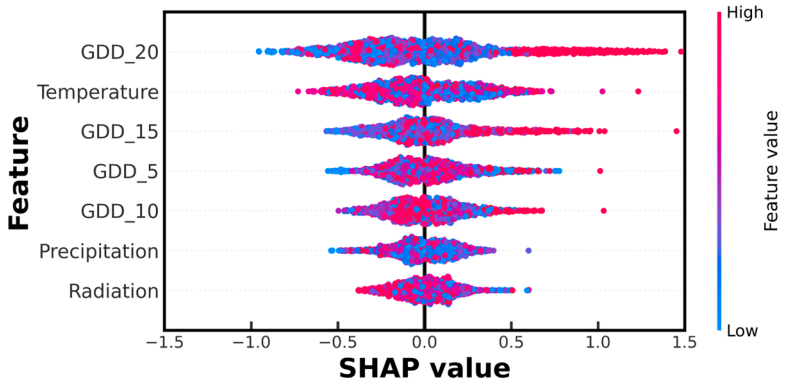


Figure 5. SHAP summary plot showing the influence of key meteorological factors on litchi yield predictions across all phenophases. The plot illustrates the SHAP values for each key meteorological factor (y-axis) in relation to litchi yield predictions. The color of each dot represents the feature value (with red indicating high values and blue indicating low values, as shown by the color bar on the right), and the horizontal position represents the SHAP value, which reflects the factor's contribution to yield prediction. GDD_X refers to Growing Degree Days with a base temperature of X °C.

3.2.2. Stage-Specific Contribution of Key Meteorological Factors

Stage-specific analysis revealed thermal dominance across all phenological phases (Figure 6). GDD_20 exhibited the highest contributions (0.300–0.345), peaking during fruit development (0.345). Mean temperature ranked second (0.158–0.196), maintaining consistent importance throughout the growth cycle. GDD_15 showed notable contributions during autumn shoot growth (0.174) and flowering (0.172), while lower thresholds (GDD_5, GDD_10) displayed minor influences (0.070–0.116). Precipitation (0.071–0.094) and radiation (0.059–0.071) exhibited weaker and more uniform contributions across stages, confirming their secondary role relative to thermal accumulation.

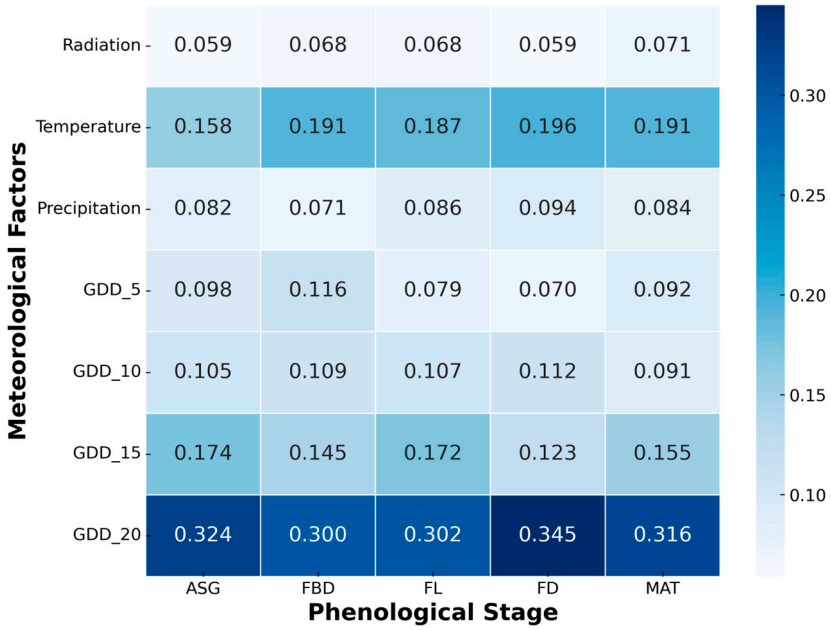


Figure 6. Contribution rates of key meteorological factors to litchi yield prediction across different phenophases. The heatmap illustrates the relative importance (contribution rate) of each meteorological factor (y-axis) during five critical growth stages (phenophases, x-axis) as determined by the Random Forest model. The values in each cell represent the contribution score, with the color intensity corresponding to the magnitude of the contribution, as indicated by the color bar. Phenophase abbreviations: ASG = autumn shoot growth, FBD = flower bud differentiation, FL = flowering, FD = fruit development, MAT = maturation.

3.2.3. Partial Dependence of Yield on Key Meteorological Factors

Partial dependence analysis revealed distinct nonlinear yield responses to meteorological variables (Figure 7). Mean temperature exhibited a positive relationship with yield in the 22–25 °C range, followed by sharp decline beyond approximately 26 °C. Accumulated thermal indices (GDD_15, GDD_20) displayed strong positive associations, with yield increasing monotonically at higher degree-day accumulations. In contrast, precipitation and radiation showed relatively flat response curves with minimal marginal effects within the observed range. These patterns indicate that thermal conditions exert stronger control on yield variability than moisture or light availability under Hainan's climate regime.

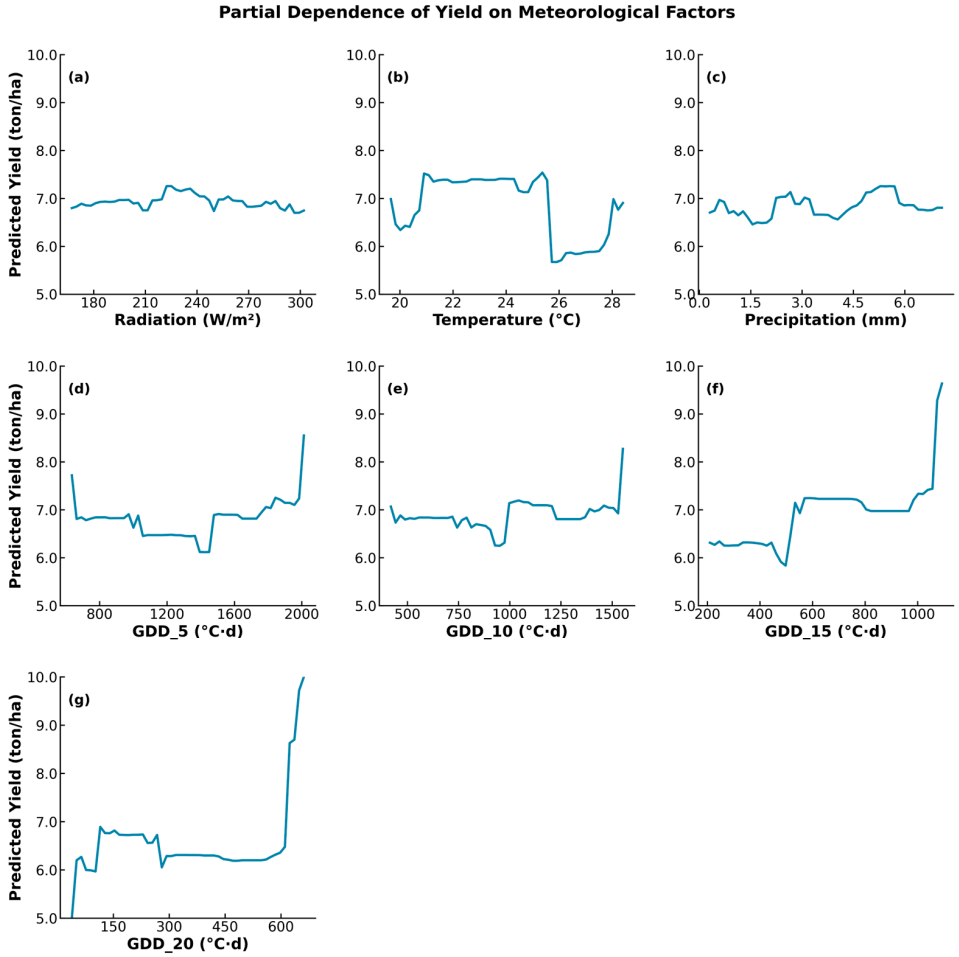


Figure 7. Partial dependence plots of meteorological factors on litchi yield: (**a**) radiation; (**b**) temperature; (**c**) precipitation; (**d**) GDD_5; (**e**) GDD_10; (**f**) GDD_15; (**g**) GDD_20, highlighting weak effects of radiation/precipitation and strong positive responses to thermal accumulation, especially GDD_20.

3.3. Sensitivity Analysis of Litchi Yield Under Climate Change Scenarios

3.3.1. Yield Response Under Different Climate Scenarios

Simulated yield trajectories under ±10% climatic perturbations (2000–2022) revealed variable sensitivities across meteorological factors (Figure 8). The analysis examined responses to systematic adjustments in temperature, precipitation, and solar radiation to assess potential impacts of climate variability on litchi production.

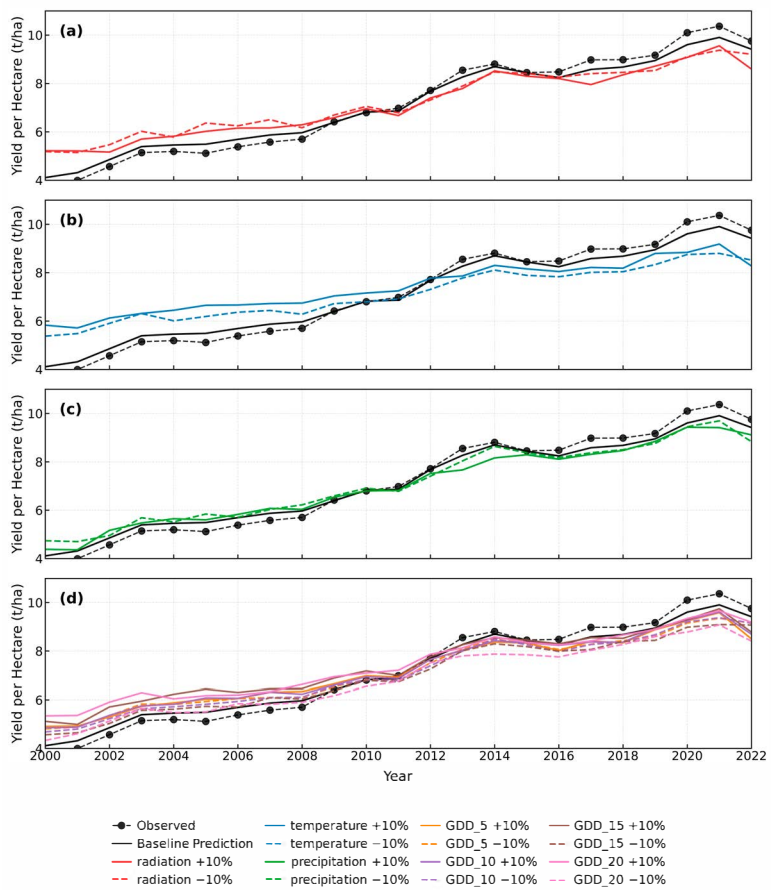


Figure 8. Sensitivity analysis of predicted litchi yield in response to ±10% changes in key meteorological variables (2000–2022). Each panel displays the simulated yield trajectories under altered scenarios for: (**a**) solar radiation, (**b**) temperature, (**c**) precipitation, and (**d**) GDD with various base temperatures. All scenarios are compared against the baseline prediction (unaltered data).

Temperature and accumulated thermal time (GDD) scenarios produced consistent directional shifts in yield. Under +10% warming, baseline yield of 4.2 t/ha in 2000 increased to approximately 5.9 t/ha, while −10% cooling reduced it to 5.4 t/ha. This pattern remained evident in subsequent years: in 2004, the baseline yield of 5.5 t/ha rose to 6.4 t/ha under warming and declined to 6.1 t/ha under cooling (Figure 8b,d). The parallel trajectories across scenarios indicate that warming scenarios generally elevated yield potential, while cooling scenarios produced reductions relative to baseline conditions.

Precipitation scenarios exhibited asymmetric yield responses. Rainfall reduction (−10%) decreased yields more substantially than surplus rainfall (+10%) increased them. In 2000, the drought scenario reduced yields to 3.9–4.0 t/ha, whereas surplus rainfall scenarios resulted in yields of approximately 4.5 t/ha—both deviating from the 4.2 t/ha baseline, but with greater magnitude under deficit conditions (Figure 8c). This pattern persisted throughout the study period, with drought scenarios consistently tracking below baseline while surplus scenarios showed modest positive deviations.

Solar radiation perturbations produced complex, variable responses. In 2000, both +10% and −10% radiation scenarios resulted in yields of approximately 5.2–5.3 t/ha, exceeding the baseline of 4.2 t/ha (Figure 8a). However, in subsequent years, radiation effects were smaller and less consistent, with trajectories converging more closely to baseline values. This variability across years suggests that radiation effects may be modulated by interactions with other climatic variables or by year-specific conditions not fully captured in isolated perturbation scenarios.

3.3.2. Sensitivity Analysis of Yield During Key Growth Periods

Stage-specific perturbation analysis revealed differential climatic sensitivities across phenological phases (Table 3). To assess vulnerability windows, meteorological variables were perturbed independently during each growth stage while holding other periods at baseline conditions. During autumn shoot growth and flower bud differentiation, warming scenarios produced positive yield responses. Temperature increase (+2 °C) elevated yields by 6.99% and 7.54%, respectively. High-threshold heat accumulation showed pronounced effects: GDD_20 + 10% increased autumn shoot growth yields by 14.93%, while GDD_20 − 10% caused minimal reduction (−1.12%). Lower threshold indices (GDD_5, GDD_10) showed weaker responses, with contributions ranging from −2.37% to +7.89%. Cooling scenarios (−2 °C) also produced positive but smaller effects (+3.90% and +3.58% for the two stages). The flowering stage showed contrasting sensitivities between thermal and hydrological factors. Warming (+2 °C) increased yields by 3.96%, while precipitation perturbations exhibited strong asymmetry: rainfall deficit (−30 mm) reduced yields by 8.09%, whereas surplus (+30 mm) provided limited benefit (+1.66%). Radiation perturbations (±60 $W \cdot m^{-2}$) produced modest positive effects (+3.01% to +3.83%), and GDD responses varied by threshold, with GDD_5 − 10% showing the largest positive contribution (+5.93%). Fruit development displayed inverse thermal responses compared to other stages. Warming (+2 °C) decreased yields (−4.26%), while cooling (−2 °C) increased them (+6.06%). Both precipitation extremes negatively impacted yields, with deficits causing greater losses (−4.51%) than surpluses (−3.00%). Radiation reduction (−60 $W \cdot m^{-2}$) increased yields (+5.21%), whereas increased radiation had minimal effect (+1.39%). GDD perturbations showed mixed effects, with higher thresholds (GDD_15, GDD_20) producing small positive responses (+1.55% to +2.80%). The maturation stage exhibited strong thermal dependence. Warming (+2 °C) increased yields by 18.35%, and GDD_20 +10% produced nearly equivalent gains (+17.97%). Conversely, GDD_20 − 10% caused substantial losses (−7.81%). Precipitation surplus (+30 mm) and radiation reduction (−60 $W \cdot m^{-2}$) also enhanced yields during this stage (+9.51% and +7.75%, respectively), while other GDD indices showed varied but generally positive contributions when increased.

Table 3. Percentage change in litchi yield in response to ±10% variations in meteorological factors across critical growth stages.

Phenophase	Temp + 2 °C (Mean ± Std)	Temp − 2 °C (Mean ± Std)	Pre + 30 mm (Mean ± Std)	Pre − 30 mm (Mean ± Std)	Rad + 60 $W \cdot m^{-2}$ (Mean ± Std)	Rad − 60 $W \cdot m^{-2}$ (Mean ± Std)	GDD_5 + 10% (Mean ± Std)
Autumn Shoot Growth	+6.99 ± 1.63	+3.90 ± 1.30	−1.37 ± 1.69	−1.40 ± 1.47	+4.41 ± 1.93	+6.66 ± 1.57	+7.92 ± 1.31
Flower Bud Differentiation	+7.54 ± 1.70	+3.58 ± 1.75	−3.88 ± 1.58	−5.10 ± 1.36	+1.96 ± 1.84	+6.83 ± 1.89	+2.98 ± 0.94
Flowering	+3.96 ± 1.72	−0.00 ± 1.31	+1.66 ± 2.26	−8.09 ± 1.88	+3.83 ± 2.32	+3.01 ± 2.57	−0.14 ± 1.09
Fruit Development	−4.26 ± 1.62	+6.06 ± 2.24	−3.00 ± 1.98	−4.51 ± 1.92	+1.39 ± 1.36	+5.21 ± 1.76	−0.23 ± 0.72
Maturity	+18.35 ± 2.43	−2.48 ± 1.64	+9.51 ± 1.59	+2.98 ± 1.83	+3.62 ± 1.47	+7.75 ± 1.62	+2.29 ± 0.69
Phenophase	**GDD_5 − 10% (mean ± std)**	**GDD_10 + 10% (mean ± std)**	**GDD_10 − 10% (mean ± std)**	**GDD_15 + 10% (mean ± std)**	**GDD_15 − 10% (mean ± std)**	**GDD_20 + 10% (mean ± std)**	**GDD_20 − 10% (mean ± std)**
Autumn Shoot Growth	−1.12 ± 0.51	+7.89 ± 1.32	−2.37 ± 0.45	+10.17 ± 1.46	−4.57 ± 0.46	+14.93 ± 2.40	−3.37 ± 0.69
Flower Bud Differentiation	+1.13 ± 0.80	+1.77 ± 0.74	+1.35 ± 0.90	+2.51 ± 1.19	+0.40 ± 0.82	+2.83 ± 0.86	−1.85 ± 0.58
Flowering	+5.93 ± 1.69	+0.52 ± 0.70	+3.43 ± 1.19	+0.28 ± 0.47	+1.06 ± 0.67	+0.87 ± 0.77	−0.67 ± 0.26
Fruit Development	+2.75 ± 0.98	−1.27 ± 0.62	+3.54 ± 1.04	+2.70 ± 1.03	+1.55 ± 0.94	+1.90 ± 1.04	+2.80 ± 1.45
Maturity	−0.27 ± 0.46	+4.45 ± 0.97	−1.53 ± 0.45	+12.11 ± 1.39	−2.19 ± 0.50	+17.97 ± 2.55	−7.81 ± 1.08

4. Discussion

4.1. Thermal Dominance and Stage-Specific Sensitivities

This study demonstrates that heat accumulation, particularly growing degree days above 20 °C (GDD_20), is the primary driver of litchi yield in Hainan. This finding aligns with established understanding of thermal time requirements in perennial fruit trees, where yield formation depends strongly on accumulated heat units [2,10,29]. The interpretable machine learning approach revealed nonlinear temperature effects: moderate warming (22–25 °C) enhanced yields, while temperatures exceeding approximately 26 °C during fruit development reduced productivity. This threshold response is consistent with physiological studies documenting thermal stress effects on net photosynthesis and respiration in litchi and other fruit crops [37,38].

Stage-specific analysis identified distinct vulnerability windows. Precipitation exhibited contrasting effects across phenological phases: drought during flowering reduced yields substantially (−8.09%), whereas moisture impacts during fruit development were bidirectional. These patterns reflect established water relations in litchi, where moisture dynamics regulate fruit quality and disease susceptibility [13,28]. Similarly, the negative warming effect during fruit development (−4.26%) contrasts with positive effects during other stages, suggesting stage-specific thermal optima that may guide targeted management interventions.

4.2. Implications for Climate Adaptation

The stage-specific sensitivities identified here suggest potential pathways for climate-smart cultivation practices. During autumn shoot growth and maturation, when thermal accumulation positively influences yields, management practices that enhance soil thermal capacity (e.g., mulching, reflective films) may prove beneficial in cooler years [39]. Conversely, the heat sensitivity observed during fruit development indicates potential value in cooling interventions such as shading nets, which have demonstrated efficacy in reducing photoinhibition and thermal stress in litchi and citrus [40,41].

The pronounced drought sensitivity during flowering (−8.09% yield reduction under −30 mm scenarios) highlights the importance of irrigation infrastructure for production stability. Complementary drainage management may mitigate waterlogging risks during fruit development, particularly given Hainan's concentrated rainy season, as root aeration constraints have been documented to compromise fruit crop yields [42]. These findings provide a framework for differentiated, phenology-aligned management strategies, though implementation feasibility will vary with farm scale and resource availability.

4.3. Model Performance and Limitations

The optimized Random Forest model achieved robust performance (R^2 = 0.564 provincially; 0.51–0.94 regionally), substantially exceeding linear baseline methods. This outcome is consistent with recent agricultural informatics studies demonstrating ensemble learning superiority in capturing nonlinear climate-yield relationships [20,43–45]. Feature importance analysis, similar to approaches in recent crop modeling work [46], provided interpretable insights into driver hierarchy while maintaining predictive accuracy.

However, spatial validation revealed systematic bias in topographically complex central-western regions (e.g., Baoting, Changjiang), where prediction errors exceeded ±0.40 t/ha. This heterogeneity likely reflects microclimate effects inadequately captured by regional meteorological stations—a recognized challenge in litchi climate suitability studies [4,47,48]. Incorporating high-resolution topographic and edaphic covariates may improve performance in these areas.

Two fundamental limitations define future research directions. First, the model assumes climate-driven yield responses without accounting for biological feedback mechanisms, notably alternate bearing. Heavy crop loads deplete carbohydrate reserves, affecting subsequent floral differentiation and introducing multi-year yield cycles not captured in single-year climate relationships [16,17]. Integrating physiological state variables (e.g., tree nutrient status, carbohydrate reserves) could improve interannual predictions.

Second, extreme stochastic events remain challenging. Catastrophic typhoons (e.g., Super Typhoon Yagi, 2024) cause mechanical damage and tree mortality that exceed the scope of statistical climate models [49]. Additionally, socioeconomic factors—particularly varietal innovation—substantially alter climate responses. Recent cultivar introductions in Hainan, including 'Lingfeng Nuo' [50], 'Tech One' [51], and 'Guizao Li' [52], exhibit distinct phenological characteristics and stress tolerances that current models do not differentiate. Future frameworks should integrate variety-specific parameters or develop hybrid approaches coupling data-driven methods with process-based crop models to capture these dynamics. Quantifying variety-specific climate resilience will be essential for evidence-based cultivar selection and breeding programs.

5. Conclusions

This study represents the first systematic quantification of the nonlinear and stage-specific responses of litchi yield to meteorological drivers in Hainan's tropical monsoon climate. By integrating a Random Forest model with interpretable machine learning (SHAP), we overcame the limitations of traditional linear approaches, achieving robust predictive capability at the provincial scale (R^2 = 0.564, RMSE = 2.1 t·ha^{-1}) and high accuracy across major production zones (R^2 = 0.51–0.94). Three critical insights emerged regarding the climate–yield dynamic:

(1) Heat accumulation is the primary determinant of yield potential. GDD_20 alone contributed 33.8% to the model's explanatory power, and thermal indices collectively explained over 85% of yield variability. This confirms that sufficient thermal time is the fundamental prerequisite for high yields in this tropical system.

(2) The scenario analysis revealed a "warming paradox" and distinct hydrological vulnerabilities. While moderate warming generally enhances yield by promoting vegetative growth and ripening, the Fruit Development stage represents a critical bottleneck where heat stress (>26 °C) triggers yield decline. Furthermore, precipitation exhibits a stark asymmetry: the yield penalty for drought during Flowering (−8.09%) far outweighs the marginal benefits of surplus rainfall, identifying this window as the most sensitive to water deficit.

(3) Evaluating stage-specific sensitivities highlights the necessity for precision adaptation strategies. To maximize the benefits of a warming climate while mitigating risks, management must pivot from uniform inputs to phenology-aligned interventions: specifically, securing irrigation during flowering to prevent pollination failure and deploying cooling technologies (e.g., shading, microsprinklers) during fruit development to alleviate thermal and photo-oxidative stress.

Despite the model's strong performance, spatial validation indicated reduced accuracy in topographically complex central-western regions, likely due to uncaptured microclimatic heterogeneity. Additionally, the current framework does not explicitly account for biological feedback loops (such as alternate bearing) or stochastic damage from super typhoons. Future research should prioritize hybrid modeling approaches that couple data-driven machine learning with biophysical process models that can simulate interannual outcomes and nutrient allocation, as well as socioeconomic factors, to overcome the shortcomings of purely statistical models in capturing biological feedback and extreme

events. Secondly, high-resolution databases encompassing variety traits, soil properties, and microtopography are needed to improve model accuracy in highly heterogeneous areas. For implementation, the findings translate to specific management practices like ensuring timely irrigation at flowering to counter drought stress. These precision, phenology-timed measures can potentially increase yields while using fewer resources than conventional uniform management. Ultimately, this study provides a theoretical foundation and actionable evidence for transitioning Hainan's litchi industry from passive weather dependence to active, climate-smart resilience.

Author Contributions: Conceptualization, L.F. and C.S.; methodology, C.S. and Z.L.; software, Z.L.; validation, R.L. and J.N.; formal analysis, L.F. and Z.L.; investigation, R.L., J.X. and M.S.; resources, L.B.; data curation, J.N.; writing—original draft preparation, L.F.; writing—review and editing, C.S. and L.B.; visualization, M.S.; supervision, C.S. and L.B.; project administration, C.S.; funding acquisition, C.S. All authors have read and agreed to the published version of the manuscript.

Funding: This research was funded by the National Natural Science Foundation of China, grant number 32260294; the Scientific Research Foundation of Hainan University, grant number KYQD(ZR)-22083 and the Natural Science Foundation of Hainan Province, grant number 423QN317 and 425RC692.

Institutional Review Board Statement: Not applicable.

Informed Consent Statement: Not applicable.

Data Availability Statement: Data are available on reasonable request to the corresponding author due to institute restriction.

Acknowledgments: We gratefully acknowledge the Hainan Intelligent Computing Center of Baiwangxin for providing the computational resources required for this study. We also sincerely thank the anonymous reviewers for their valuable and constructive comments.

Conflicts of Interest: The authors declare no conflict of interest.

Abbreviations

The following abbreviations are used in this manuscript:

GDD	Growing Degree Days
SHAP	SHapley Additive exPlanations
MLR	Multiple Linear Regression
RF	Random Forest
GBDT	Gradient Boosting Decision Trees
ET	Extreme Random Trees
KNN	K-Nearest Neighbors
CV	Cross-Validation
OOF	out-of-fold
FBD	flower bud differentiation
FL	flowering
FD	fruit development
MAT	maturation
ASG	autumn shoot growth

Appendix A. Supplementary Correlation Analysis

Appendix A.1. Spatiotemporal Heterogeneity in Climate and Litchi Yield

A foundational challenge in predicting litchi yield in Hainan Province lies in the significant heterogeneity of its climatic endowments and the dynamic evolution of its agricultural production systems. Analysis of long-term meteorological data reveals distinct

and complex spatial patterns (Figure A1). The thermal regime is primarily dictated by topography, creating a center-outward gradient with cooler temperatures in the central highlands and uniformly high temperatures along the coastal lowlands (Figure A1a). Precipitation, in contrast, shows a clear east–west divide, with the highest rainfall concentrated in the eastern and southeastern regions (Figure A1b). Critically, solar radiation does not follow either pattern, with the highest levels found in the western and northeastern areas (Figure A1c). Concurrently, the geography of litchi production has undergone a dramatic transformation (Figure A6). While yields were low and diffusely distributed in the early 2000s (Figure A6a), a clear pattern of intensification emerged over the subsequent decades, culminating in the establishment of dominant, high-yield hubs in the northeastern regions, particularly Wenchang and Qionghai (Figure A6b–d). The evident spatial mismatch is striking: the highest-yielding zones are not located in the warmest or wettest areas. Instead, it seems that they emerged in an agro-climatic 'sweet spot', characterized by high levels of solar radiation and moderate, non-excessive precipitation. This complex interplay underscores the limitations of simple spatial correlation and highlights the necessity of a more sophisticated modeling approach to deconstruct the drivers of litchi yield.

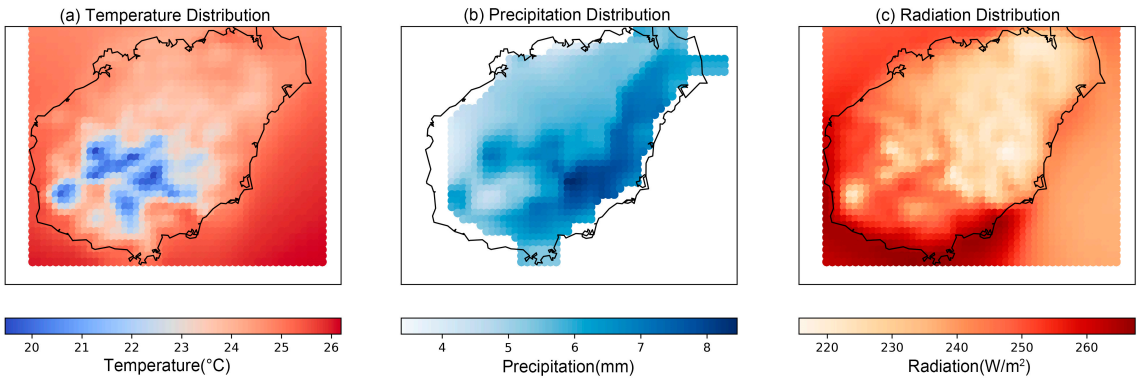


Figure A1. Spatial distribution of key mean annual agroclimatic variables across Hainan's major litchi-growing regions from 2000 to 2022. The maps display the spatial patterns for (**a**) mean annual temperature (°C), (**b**) mean daily precipitation (mm), and (**c**) mean daily solar radiation (MJ/m^2).

The influence of meteorological factors is highly dependent on the crop's phenological stage. As illustrated in Figure A2, the correlation analysis reveals distinct and sometimes opposing roles for key climate variables across the growing season. The most prominent pattern is the "U-shaped" importance of thermal conditions. Factors related to heat, including temperature and all GDD indices, exhibit their strongest positive correlation with final yield at the two ends of the season. They are critical during the initial Bud Sprout Period ($r \approx 0.39$) and again during the final Maturation Period ($r = 0.40$). In contrast, their correlation is substantially weaker during the intermediate stages. The roles of precipitation and radiation present a stark contrast. Precipitation shifts from a negligible influence during the early stages to a significant negative correlation during Fruit Development ($r = -0.22$) and Maturation ($r = -0.24$). This suggests that excessive rainfall late in the season is detrimental, likely due to increased disease pressure or fruit splitting. Conversely, solar radiation emerges as the most critical factor during the Maturation Period ($r = 0.43$), highlighting that ample sunlight is paramount for developing high-yield fruit. Its negative correlation during Flower Bud Differentiation ($r = -0.22$) points to a more complex, non-linear role. This complexity provides a strong rationale for employing machine learning models, which can capture these intricate, non-linear relationships. The detailed monthly correlation patterns for four representative regions, which illustrate these complex relationships, are presented in Appendix B.2 (Figure A5).

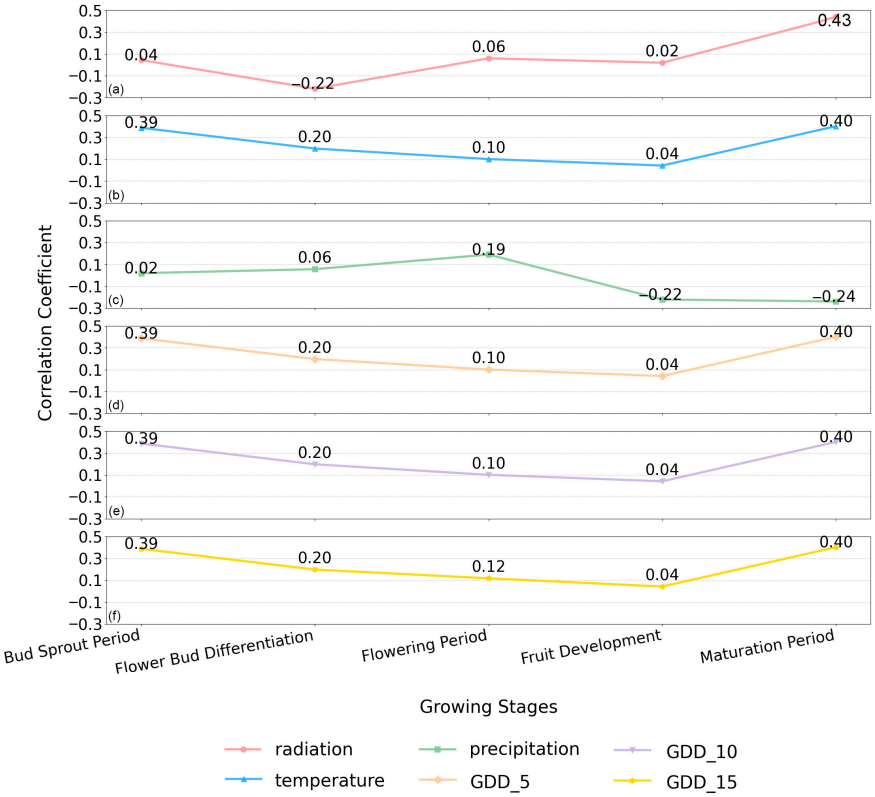


Figure A2. Correlation coefficients between key meteorological factors and litchi yield across five critical phenological stages: (**a**) radiation; (**b**) temperature; (**c**) precipitation; (**d**) GDD_5; (**e**) GDD_10; (**f**) GDD_15. The plot shows the Pearson correlation coefficients between provincial average yield and meteorological variables aggregated by stage. GDD_5, GDD_10, and GDD_15 represent Growing Degree-Days calculated with base temperatures of 5 °C, 10 °C, and 15 °C, respectively.

Appendix A.2. Quantitative Analysis of Monthly Climate-Yield Correlations

During the Autumn Shoot Growth Period (August–October), temperature and GDD indices generally exhibit a significant positive correlation with yield. In Lingao (Figure A3a) and Tunchang (Figure A3b), the correlation coefficients (r) during this stage range from 0.23 to 0.73, with the GDD_15 correlation in Tunchang for August reaching as high as r = 0.73. Conversely, precipitation from August to September is predominantly negatively correlated with yield (R-values between −0.24 and −0.21), indicating that excessive rainfall during this period may be unfavorable for yield formation. The correlation patterns shift during the Flower Bud Differentiation Period (November–January), when the relationship with temperature weakens and, in some months, becomes negative in regions like Chengmai (Figure A3c) and Lingshui (Figure A3d). Notably, solar radiation also shows a consistent negative correlation in November and December, with R-values ranging from −0.20 to −0.03. This quantitative result clearly indicates that lower winter temperatures and relatively weaker solar radiation are favorable conditions for promoting litchi flower bud differentiation. Finally, during the critical period of fruit development and maturation (April–July), nearly all meteorological factors shift to a strong positive correlation. Across all four regions, the correlations for temperature and GDDs peak during this stage, with coefficients commonly exceeding 0.50. For instance, the GDD_15 correlation in Chengmai (Figure A3c) for April reached the highest value observed in the entire study (r = 0.78), while the temperature correlation in Lingshui (Figure A3d) for July also reached r = 0.55, quantitatively highlighting the critical importance of favorable light and thermal conditions during this stage for determining the final yield. The correlation patterns for the remaining

13 production regions are provided in Appendix B.2 (Figure A5) for a comprehensive regional comparison.

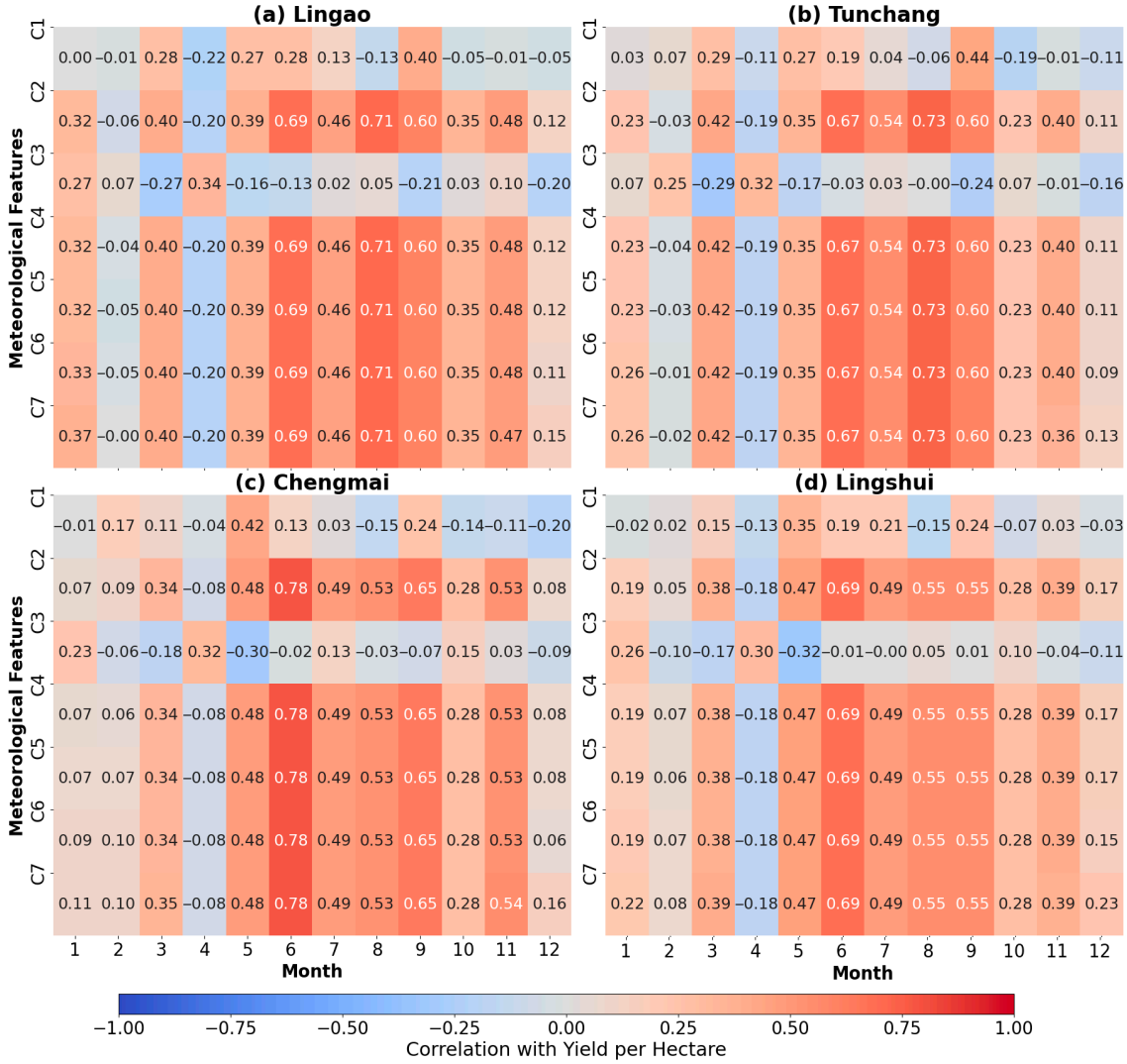


Figure A3. Correlation heatmaps between monthly meteorological factors and yield per ha for four major litchi production regions: (**a**) Lingao, (**b**) Tunchang, (**c**) Chengmai, and (**d**) Lingshui.

Appendix B. Background Trends in Climate and Litchi Cultivation

Appendix B.1. Long-Term Regional Climate Trends (2000–2022)

Analysis of long-term meteorological data from 2000 to 2022 reveals significant climatic shifts in Hainan's litchi production regions. As shown in Figure A4, there has been a consistent warming trend, with the annual average temperature rising from 24.0 °C in 2000 to 25.2 °C in 2022, at an approximate rate of 0.055 °C per year (Figure A4a). In contrast, annual precipitation has shown high interannual variability without a significant linear trend (Figure A4b). Annual solar radiation has exhibited a slight but steady increase, from 240 MJ/m^2 to 250 MJ/m^2 over the 22-year period (Figure A4c). These background climatic changes form a critical context for understanding litchi yield dynamics.

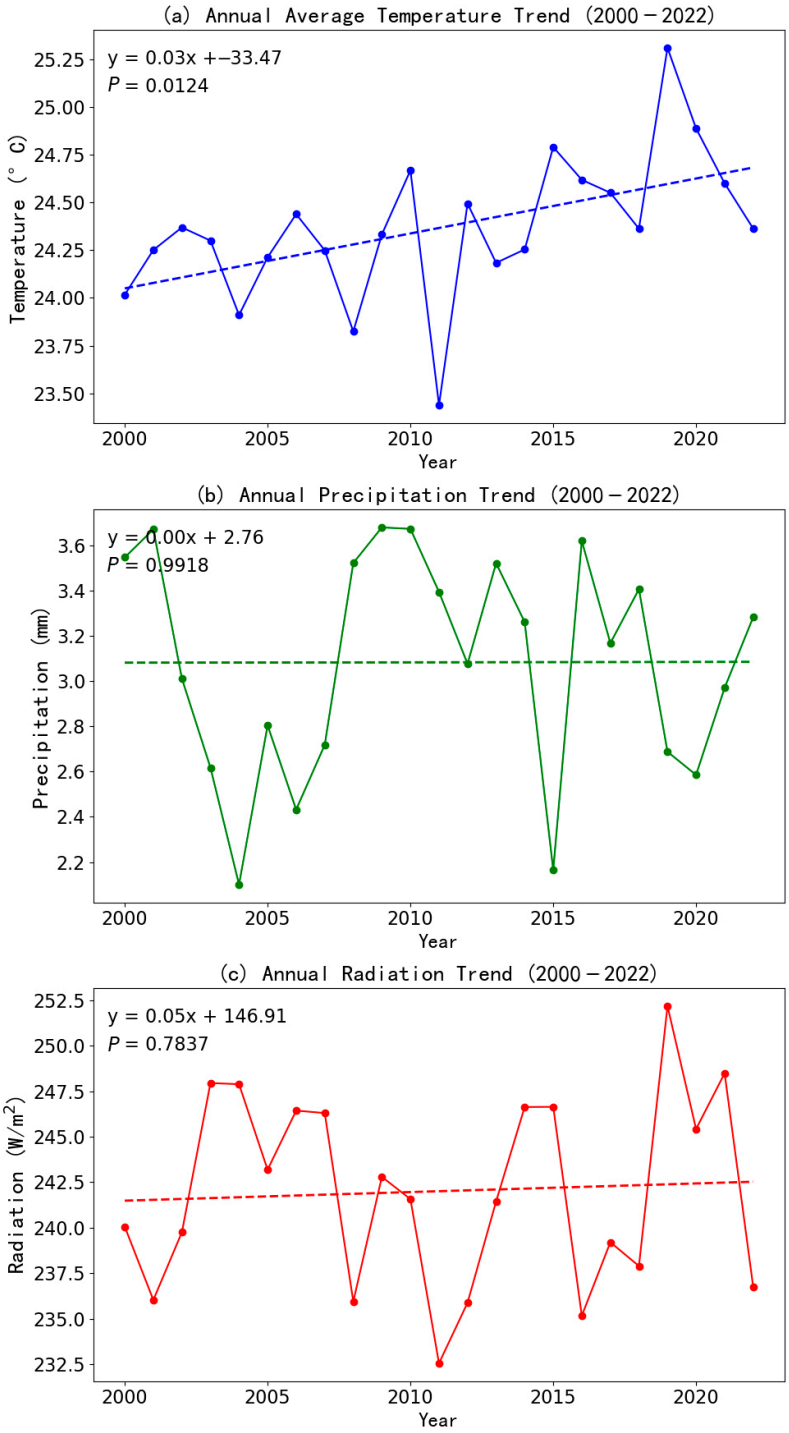


Figure A4. Long-term trends in annual mean meteorological factors in Hainan's litchi production areas (2000–2022): (**a**) Temperature, (**b**) Precipitation, and (**c**) Solar Radiation.

Appendix B.2. Supplementary Correlation Analysis

Figure A5 provides supplementary heatmaps illustrating the Pearson correlation coefficients between key meteorological factors and litchi yield across five phenological stages for 13 additional production regions in Hainan Province. The data detail the quantitative relationships for variables including solar radiation, temperature, precipitation, and GDD indices. This detailed regional breakdown is intended to facilitate more nuanced comparative analyses of localized climate-yield dynamics.

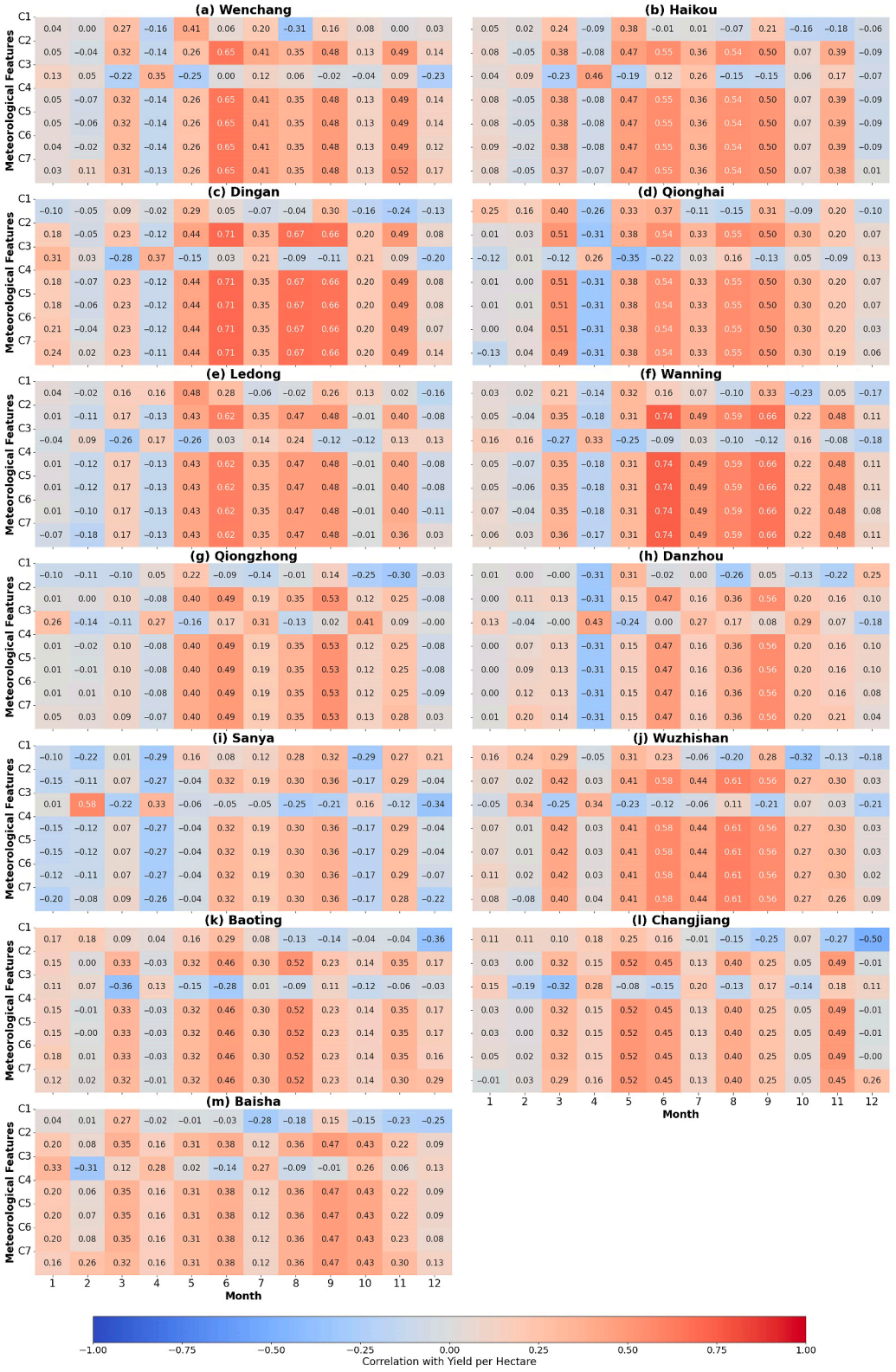


Figure A5. Correlation coefficient heatmaps for 13 additional litchi production regions in Hainan Province. (Correlation heatmaps of meteorological variables with litchi yield across regions. For clarity, meteorological variables are abbreviated as: C1 = radiation, C2 = temperature, C3 = precipitation, C4 = GDD_5, C5 = GDD_10, C6 = GDD_15, C7 = GDD_20).

Appendix B.3. Spatiotemporal Evolution of Litchi Cultivation Area (2000–2022)

The spatial distribution of Hainan's litchi industry underwent a significant transformation between 2000 and 2022, shifting from dispersed cultivation to geographically concentrated production hubs (Figure A6). Initially, during 2000–2004, the harvested area was centered in traditional regions like Haikou (530.8 ha) and Qionghai (558.2 ha), which together constituted 38.7% of the provincial total (Figure A6a). This spatial reorganization began to take shape during 2005–2010, with a noticeable expansion of cultivation in northeastern areas (Figure A6b). Over the subsequent decades, a clear trend of spatial agglomeration emerged, particularly in the northeastern part of the province. This trend intensified significantly by 2011–2014, when Haikou's harvested area expanded to 3918.8 ha (Figure A6c). In the most recent period (2015–2022), Haikou solidified its status as the dominant production center, with its harvested area reaching 5199.6 ha and accounting for 26.3% of the provincial total (Figure A6d).

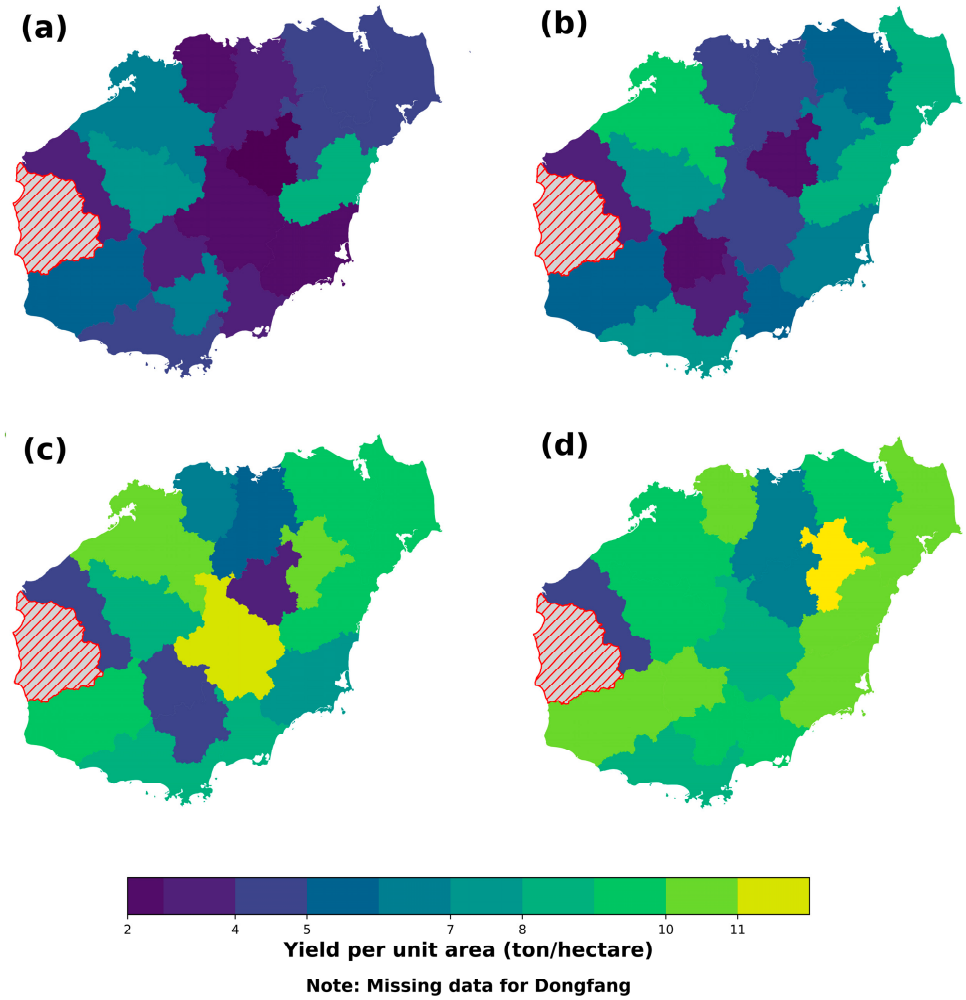


Figure A6. Spatiotemporal evolution of litchi yield per unit area (t/ha) in Hainan Province across four distinct time periods: (**a**) 2000–2004, (**b**) 2005–2010, (**c**) 2011–2014, and (**d**) 2015–2022.

Appendix C. Supplementary Prediction Results Under Extreme Climate Scenarios

Table A1 presents supplementary prediction results for litchi yield under more extreme climate scenarios. The following Table A1 details the predicted yields (in t/ha) for each major production region when meteorological factors during specific phenological stages are altered by ±30%. This dataset expands upon the ±10% analysis in the main text,

enabling a more comprehensive assessment of regional sensitivity and vulnerability to significant climate variations.

Table A1. Predicted litchi yield (t/ha) under simulated ±25% variations in key meteorological factors during different phenological stages.

City/County	Phenological Period	Baseline	T − 30%	T + 30%	Pre − 30%	Pre + 30%	Rad − 30%	Rad + 30%
Wanning	Autumn shoot growth period	6.98	7.22	7.60	7.07	6.79	7.30	7.10
	Flower bud differentiation period	6.86	7.24	6.80	6.93	6.67	7.28	6.97
	Flowering period	7.08	7.04	6.85	7.07	6.89	6.97	7.24
	Fruit development period	7.11	7.37	7.02	6.90	6.89	7.29	7.05
	Maturity period	6.97	7.02	7.98	6.87	7.38	7.18	7.02
Sanya	Autumn shoot growth period	7.16	7.28	7.26	7.28	7.00	7.24	7.27
	Flower bud differentiation period	7.12	7.58	7.00	7.14	6.97	6.96	7.37
	Flowering period	7.23	7.32	7.04	7.00	7.12	7.32	7.39
	Fruit development period	7.51	7.58	7.21	7.38	7.26	7.74	7.37
	Maturity period	7.29	7.18	7.73	7.28	7.47	7.25	7.39
Changjiang	Autumn shoot growth period	4.61	4.79	4.95	4.63	4.52	4.95	4.61
	Flower bud differentiation period	4.47	4.62	4.54	4.41	4.46	4.75	4.48
	Flowering period	4.25	4.21	4.39	4.22	4.24	4.33	4.31
	Fruit development period	4.39	4.49	4.79	4.31	4.35	4.45	4.53
	Maturity period	4.69	4.66	5.11	4.60	4.82	4.85	4.71
Dingan	Autumn shoot growth period	8.36	8.47	9.11	8.37	8.31	8.37	8.38
	Flower bud differentiation period	8.49	8.39	8.58	8.61	8.29	9.29	8.32
	Flowering period	8.46	8.24	8.18	8.40	8.31	8.46	8.79
	Fruit development period	8.18	8.35	8.19	8.13	7.94	8.27	7.98
	Maturity period	8.20	8.23	9.30	7.97	8.81	8.82	7.90
Baisha	Autumn shoot growth period	8.12	8.12	8.60	8.11	8.08	8.18	8.00
	Flower bud differentiation period	8.15	8.24	8.11	8.20	8.12	8.26	8.20
	Flowering period	7.99	7.99	7.80	8.05	7.89	8.01	7.90
	Fruit development period	8.08	8.22	8.06	7.86	8.08	8.27	7.77
	Maturity period	8.00	7.92	8.67	7.80	8.29	8.50	7.58
Chengmai	Autumn shoot growth period	5.76	5.91	6.28	5.81	5.68	6.08	5.80
	Flower bud differentiation period	5.65	5.93	5.60	5.62	5.64	5.96	5.75
	Flowering period	5.69	5.71	5.56	5.71	5.58	5.80	5.74
	Fruit development period	5.43	5.59	5.66	5.38	5.30	5.61	5.61
	Maturity period	5.95	5.83	6.63	5.95	6.15	6.16	6.14
Lingao	Autumn shoot growth period	6.90	7.30	7.55	7.00	6.71	7.26	7.00
	Flower bud differentiation period	6.95	7.02	6.83	6.93	6.83	7.38	7.19
	Flowering period	6.70	6.60	6.36	6.66	6.51	6.56	6.73
	Fruit development period	6.60	6.89	6.38	6.46	6.38	6.87	6.57
	Maturity period	6.69	6.79	7.82	6.57	7.10	7.12	6.68
Tunchang	Autumn shoot growth period	4.40	4.63	5.21	4.48	4.31	4.56	4.65
	Flower bud differentiation period	4.42	4.62	4.68	4.45	4.31	4.88	4.47
	Flowering period	4.28	4.27	4.56	4.39	4.16	4.29	4.74
	Fruit development period	4.21	4.69	4.73	4.18	4.17	4.33	4.32
	Maturity period	4.70	4.77	5.80	4.60	5.03	4.97	4.95
Wenchang	Autumn shoot growth period	8.00	8.11	8.54	7.99	7.80	8.08	8.08
	Flower bud differentiation period	8.15	8.40	7.99	8.21	7.99	8.31	8.37
	Flowering period	8.28	8.50	7.91	8.37	8.08	8.07	8.45
	Fruit development period	8.04	8.38	7.80	7.86	7.79	8.17	8.11
	Maturity period	8.24	7.98	9.05	8.18	8.52	8.32	8.48
Lingshui	Autumn shoot growth period	7.13	7.37	7.77	7.09	7.04	7.40	7.13
	Flower bud differentiation period	7.15	7.35	7.15	7.15	7.01	7.51	7.45
	Flowering period	7.12	7.07	6.92	7.12	6.95	7.16	7.13
	Fruit development period	7.22	7.29	7.10	7.14	6.97	7.36	7.10
	Maturity period	7.08	7.04	8.15	6.97	7.54	7.31	7.10
Ledong	Autumn shoot growth period	7.49	7.42	8.19	7.45	7.37	7.47	7.80
	Flower bud differentiation period	7.44	7.56	7.39	7.36	7.40	7.73	7.53
	Flowering period	7.80	7.85	7.38	7.81	7.55	7.64	7.89
	Fruit development period	7.70	7.78	7.55	7.54	7.39	7.55	7.91
	Maturity period	7.66	7.46	8.65	7.55	8.05	7.76	7.77
Haikou	Autumn shoot growth period	7.24	7.43	7.83	7.36	7.05	7.55	7.24
	Flower bud differentiation period	7.04	7.39	7.15	7.13	6.90	7.37	7.26
	Flowering period	7.33	7.27	7.17	7.30	7.13	7.43	7.45
	Fruit development period	7.30	7.50	7.32	7.06	7.07	7.39	7.31
	Maturity period	7.27	7.20	8.37	7.11	7.76	7.56	7.20

Table A1. *Cont.*

City/County	Phenological Period	Baseline	T − 30%	T + 30%	Pre − 30%	Pre + 30%	Rad − 30%	Rad + 30%
Qiongzhong	Autumn shoot growth period	6.72	6.97	7.59	6.70	6.76	6.92	6.75
	Flower bud differentiation period	6.98	7.53	6.83	7.02	6.89	7.47	6.99
	Flowering period	7.27	7.29	6.71	7.23	7.10	7.64	7.11
	Fruit development period	6.92	7.34	6.92	6.72	6.73	7.12	6.84
	Maturity period	7.19	7.09	8.14	6.86	7.91	7.42	7.15
Qionghai	Autumn shoot growth period	8.73	8.77	8.96	8.64	8.66	8.78	8.80
	Flower bud differentiation period	8.90	8.97	8.76	8.83	8.88	8.69	9.17
	Flowering period	8.79	8.86	8.72	8.75	8.77	8.59	8.93
	Fruit development period	8.96	8.93	8.72	8.97	8.78	8.95	8.82
	Maturity period	8.58	8.53	8.97	8.58	8.69	8.74	8.55
Wuzhishan	Autumn shoot growth period	6.18	6.45	7.24	6.34	6.06	6.91	6.30
	Flower bud differentiation period	5.65	5.55	6.24	5.58	5.58	6.64	5.76
	Flowering period	5.93	5.75	6.22	6.03	5.73	5.87	6.23
	Fruit development period	5.93	6.15	7.07	5.64	5.74	5.94	5.92
	Maturity period	6.22	6.34	7.90	6.34	6.49	6.77	6.25
Danzhou	Autumn shoot growth period	8.46	8.45	8.80	8.44	8.45	8.72	8.51
	Flower bud differentiation period	8.70	9.10	8.48	8.69	8.64	8.72	8.88
	Flowering period	8.60	8.81	8.36	8.50	8.58	8.48	8.71
	Fruit development period	8.61	8.80	8.23	8.38	8.55	8.75	8.58
	Maturity period	8.72	8.43	9.02	8.43	9.05	8.63	8.74
Baoting	Autumn shoot growth period	6.89	7.29	7.36	6.99	6.60	7.66	6.96
	Flower bud differentiation period	6.94	7.14	7.40	6.91	6.81	7.53	7.12
	Flowering period	6.83	6.74	7.45	6.92	6.67	6.50	6.93
	Fruit development period	6.76	6.98	7.11	6.76	6.52	7.05	6.80
	Maturity period	7.07	7.02	7.92	7.13	7.06	7.01	7.45
Dongfang	Missing data							

Appendix D. Supplementary Model Performance Result

Appendix D.1. Spatial Validation for Symbolic Regions

The Random Forest model demonstrated consistently high performance across all six sampling areas in Hainan (see Figure A7), with coefficients of determination (R^2) ranging from 0.89 to 0.94. The best-fitting results were observed in Wanning (Figure A7a; R^2 = 0.94, RMSE = 0.80 t/ha), with Lingshui and Haikou producing similar results (Figure A7c,d; R^2 = 0.92–0.90, RMSE = 0.85). These results highlight the strong relationship between meteorological characteristics and yield in these regions. Lingao and Wenchang (Figure A7b,e) also performed well (R^2 = 0.94 and 0.89, respectively; RMSE = 1.19 and 1.01 t/ha), although the data distribution in these areas was more dispersed. Of the six locations, Ding'an showed the weakest performance (Figure A7f; R^2 = 0.89, RMSE = 1.45 t/ha). Its fitted line (y = 0.67x + 2.44) exhibited systematic bias, underestimating yields at higher production levels and overestimating them at lower ones. Notably, all panel slopes were less than one with positive intercepts (slopes: 0.67–0.82; intercepts: 1.28–2.44), reflecting a general mean-reverting trend. This is likely due to the limited availability of extreme yield data and the omission of region-specific management practices or microclimatic influences. Overall, the model demonstrates strong generalization capability but could benefit from bias correction or local fine-tuning, particularly in central regions such as Ding'an. Accuracy declines in more heterogeneous environments, particularly in the western and central mountainous areas, likely due to complex microclimates or unaccounted variations in cultivation practices. Detailed time-series and scatter plot validation results for the remaining 11 regions are presented in Appendix D.3 (Figure A9).

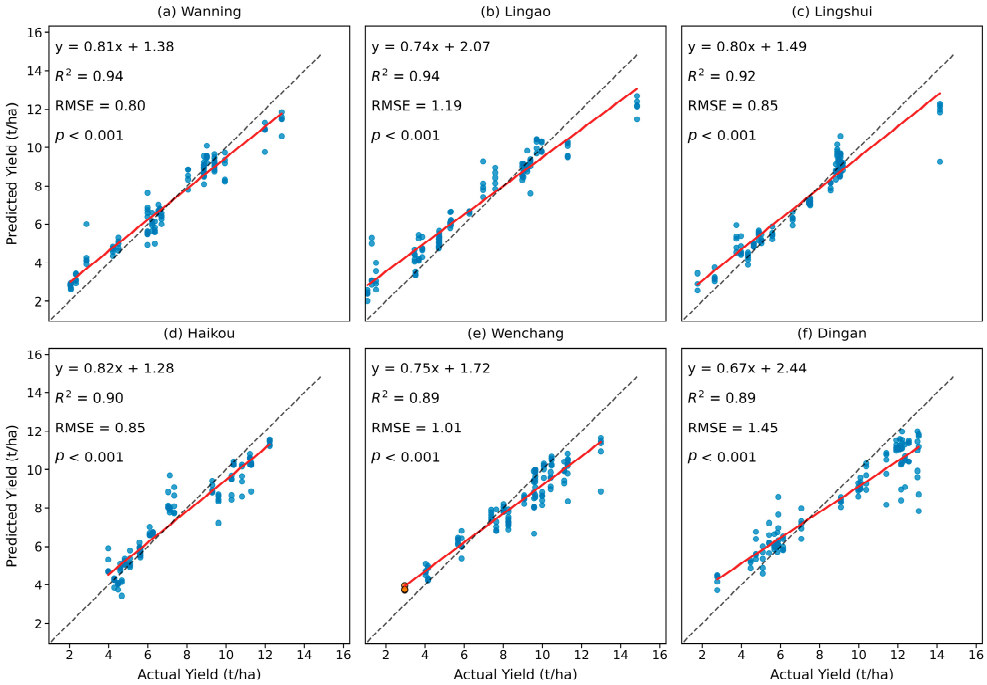


Figure A7. Spatial validation of the Random Forest model for litchi yield prediction in selected regions. The scatter plots show actual yield vs. model-predicted yield (t/ha).

Appendix D.2. Relative Importance of Meteorological Features

Collectively, the four GDD indices accounted for 85.3% of total feature importance (cumulative contribution: 0.853), far exceeding precipitation (0.125) and radiation (0.117). This hierarchy remained consistent across evaluation methods, with strong correlation between Gini-based importance and mean |SHAP| values (Spearman's ρ = 0.816, $p < 0.01$).

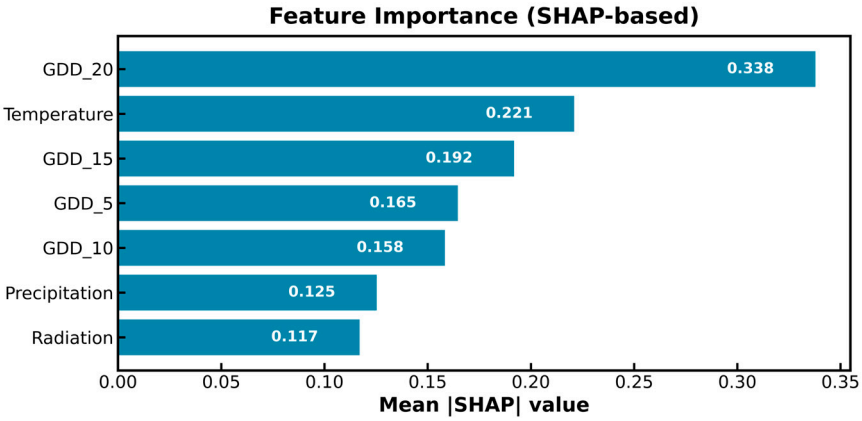


Figure A8. Relative importance of meteorological features for predicting litchi yield. The bar chart displays the importance scores for each meteorological variable as calculated by the Random Forest model, based on the Gini impurity metric.

Appendix D.3. Spatial Validation for the Remaining 11 Regions

Notably, an outlier is observed in the validation plot (Figure A9) for Figure A9g Sanya: The outlier (actual yield ≈ 12 t/ha, predicted yield ≈ 8 t/ha) corresponds to 2019 data. This deviation is primarily attributed to two factors: (1) Local variety replacement in Sanya that year (from 'Feizixiao' to 'Guizao Li', a high-yield early-ripening cultivar [52]); (2) Extreme short-term precipitation during the flowering period (February–March 2019), which was 45% above the long-term average, while local orchards adopted drip irrigation to mitigate

water stress—these management and climatic anomalies were not fully captured by the climate-driven model [31,52]. Layout adjustment: The horizontal (hspace) and vertical (wspace) spacing between subplots was adjusted to 0.2 (from the original 0.5) to optimize layout compactness. Regarding regional patterns, regions with $R^2 < 0.7$ (e.g., Wuzhishan, Baisha, Changjiang) are concentrated in the central-western mountainous areas, which aligns with the spatial distribution of prediction errors in Figure A10 (central-western regions show severe underestimation).

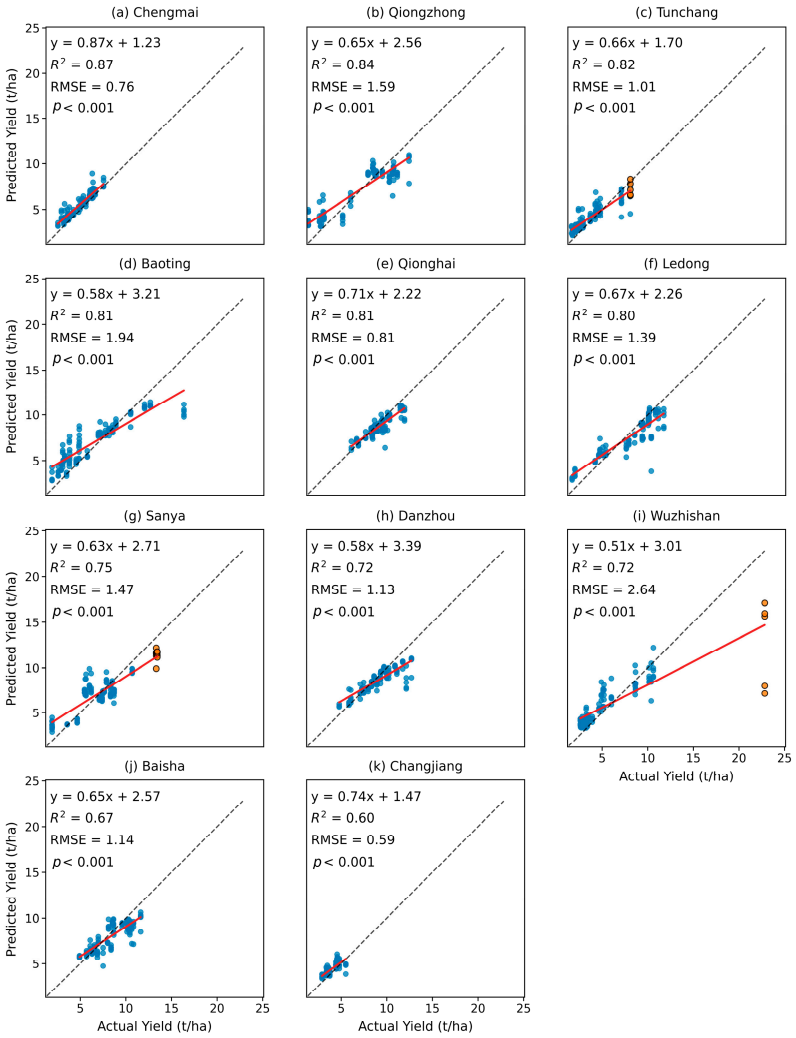


Figure A9. Supplementary spatial validation of the Random Forest model for the remaining 11 regions. The plots show actual versus model-predicted yield (t/ha). Each subplot includes the linear regression equation, coefficient of determination (R^2), *p*-value, and Root Mean Square Error (RMSE) to quantitatively assess the model's predictive performance in each specific region. Axes and units: All subplots use the same coordinate system, with the *x*-axis representing actual yield and the y-axis representing predicted yield (both in t/ha). Regression metrics: The linear equation (y = ax + b) describes the relationship between predicted and actual yields, where a (slope) reflects the model's bias (slopes < 1 indicate general underestimation of high yields, consistent with Section 3.2.2) and b (intercept) represents the baseline offset. R^2 (coefficient of determination) quantifies the model's explanatory power; RMSE (Root Mean Square Error) measures the average prediction deviation; and $p < 0.001$ confirms the statistical significance of the regression.

Appendix D.4. Temporal Analysis for the Remaining 11 Regions

Consistent with the findings in the main text, these results show the model effectively captures long-term productivity trends. The precision in predicting interannual fluctua-

tions, however, varies, with some regions (e.g., Changjiang, R^2 = 0.25) showing poorer ability to explain interannual variance. Note for Figure A10k Changjiang: The notably lower coefficient of determination (R^2 = 0.25) in Changjiang compared to other regions ($R^2 \geq 0.60$) is primarily attributed to two interrelated factors, consistent with the model limitations outlined in Section 4: (1) Microclimatic heterogeneity induced by topography: Changjiang is located in the western coastal hilly region of Hainan, where fragmented valleys and coastal aeolian landforms create localized microclimates (e.g., variable temperature gradients and uneven precipitation distribution). The current model relies on data from regional meteorological stations (Figure 1), which cannot fully capture these fine-scale environmental variations, leading to mismatches between predicted and actual yields. (2) Unrecorded management variability: Field investigations (unpublished agricultural extension data) indicate that Changjiang's litchi cultivation involves mixed cultivars (e.g., 'Feizixiao' and local low-chill varieties) and irregular irrigation practices (due to seasonal water scarcity). These management factors, which were not incorporated into the model predictors (Section 2.2), introduce additional yield variability that the climate-driven model cannot explain.

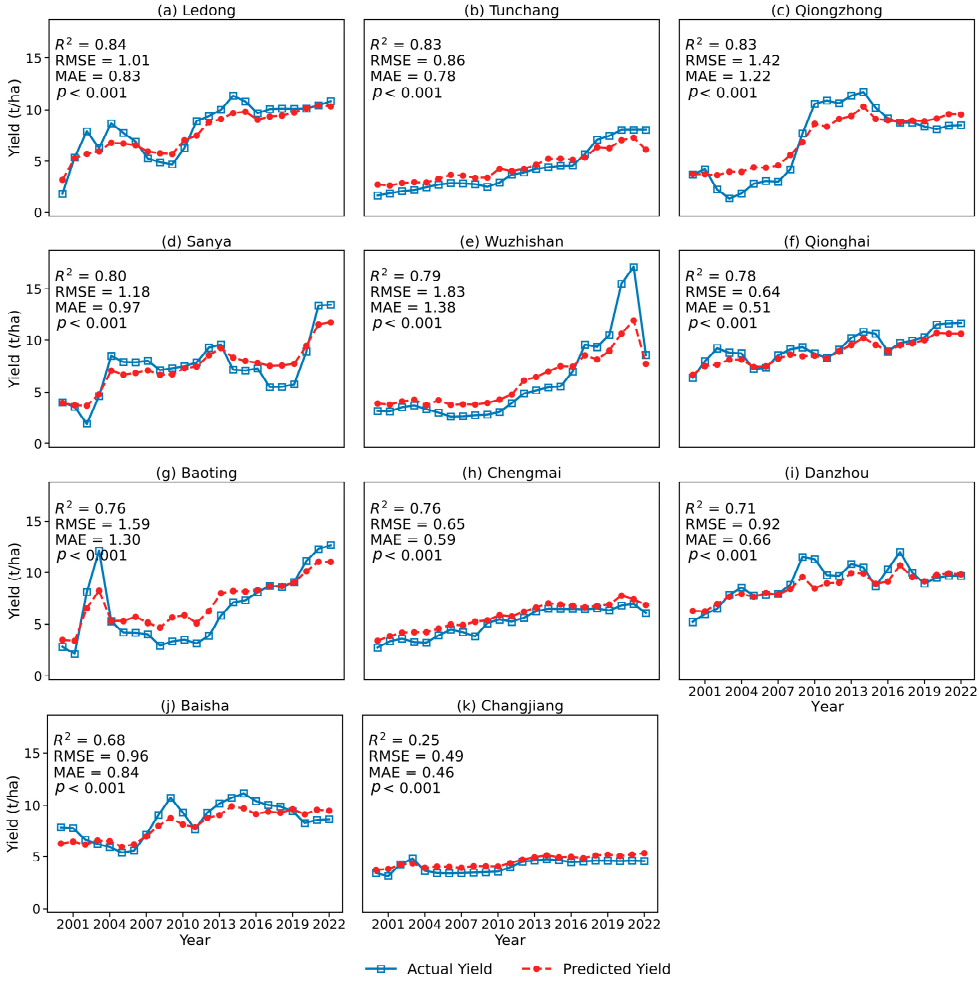


Figure A10. Supplementary temporal analysis of observed vs. predicted litchi yields for the remaining 11 regions (2001–2022). The plots compare actual yield (blue solid line) with model-predicted yield (red dotted line).

References

1. Raz, A.; Goldway, M.; Sapir, G.; Stern, R.A. "Hong Long" Lychee (*Litchi chinensis* Sonn.) Is the Optimal Pollinizer for the Main Lychee Cultivars in Israel. *Plants* **2022**, *11*, 1996. [CrossRef]
2. Tan, Z.K.; He, Y.; Ou, Z.R.; Qiu, S.J.; Wei, R.Y. The Relationship between the Development Process of "Heli" Lychee Fruits and Temperature Conditions. *Weather* **2006**, 96–101.
3. Nath, V.; Pandey, S.D.; Pongener, A.; Srivastava, K.; Marboh, E.S. Challenges and opportunities for improved productivity of litchi. *Acta Hortic.* **2018**, *1211*, 161–164. [CrossRef]
4. Kumar, G.; Nath, V.; Mandal, U.; Sena, D.R.; Pongener, A.; Ranjan, R.; Madhu, M. Climate and soil suitability zonation for Litchi (*Litchi chinensis*) in India using geo-science tool-based analytical hierarchy process. *Egypt. J. Remote Sens. Space Sci.* **2023**, *26*, 581–594. [CrossRef]
5. Gopal Kumar, G.K.; Girja Tewari, G.T.; Vinod Kumar, V.K.; Pandey, S.D.; Vishal Nath, V.N. Climate resilience in litchi (*Litchi chinensis*) orchards in Bihar through soil manipulations. *Indian J. Soil Conserv.* **2018**, *46*, 190–198.
6. Singh, H.C.P.; Rao, N.K.S.; Shivashankar, K.S.; Sharma, J. *Climate-Resilient Horticulture: Adaptation and Mitigation Strategies*; Springer: Berlin/Heidelberg, Germany, 2013.
7. Xu, N.; Qin, X.-Q.; Li, D.-B.; Hou, Y.-J.; Fang, C.; Zhang, S.-W.; You, J.-Y.; Li, H.-L.; Qiu, H.-Y. Comparative transcriptome and metabolome profiles of the leaf and fruits of a Xianjinfeng litchi budding mutant and its mother plant. *Front. Genet.* **2024**, *15*, 1360138. [CrossRef] [PubMed]
8. Zhang, H.N.; Su, Z.X.; Chen, H.B. A Comparison of Photosynthetic Characteristics of Three Lychee Varieties at Full Bloom. *J. South China Agric. Univ.* **2017**, *38*, 43–47.
9. Le, L.M.; Nguyen, T.C.; Pham, B.T.; Ly, H.-B.; Le, V.M.; Le, T.-T. Development and Identification of Working Parameters for a Lychee Peeling Machine Combining Rollers and a Pressing Belt. *AgriEngineering* **2019**, *1*, 550–566. [CrossRef]
10. Kumar, R. Effect of climate change and climate variable conditions on litchi (*Litchi chinensis* Sonn.) productivity and quality. In Proceedings of the IV International Symposium on Lychee, Longan and Other Sapindaceae Fruits, White River, South Africa, 2–6 December 2012; Volume 1029, pp. 145–154.
11. Solo, N.; Ramanankierana, H.; Miasa, E.; Donno, D.; Baohanta, R.; Rakotoniaina, E.; Soifoini, T.; Giacoma, C.; Beccaro, G. Effects of seasonal climatic variations on physiology and phenology of *Litchi chinensis* Sonn. in Madagascar. *Fruits* **2019**, *74*, 97–109. [CrossRef]
12. Goenaga, R.; Marrero, A.; Pérez, D. Growth and Nutrient Concentration of Lychee Grown on an Acid Ultisol. *HortTechnology* **2022**, *32*, 552–558. [CrossRef]
13. Kumar, G.; Kumar, R.; Nath, V.; Pande, S.; Marboh, E.; Kumar, P. Integrated Soil Management Technique for Young Growing Orchards of Litchi (*Lychee chinensis*). *Int. J. Curr. Microbiol. App. Sci* **2018**, *7*, 710–722. [CrossRef]
14. Shen, J.; Xiao, Q.; Qiu, H.; Chen, C.; Chen, H. Integrative effect of drought and low temperature on litchi (*Litchi chinensis* Sonn.) floral initiation revealed by dynamic genome-wide transcriptome analysis. *Sci. Rep.* **2016**, *6*, 32005. [CrossRef] [PubMed]
15. Paireau, J.; Tuan, N.H.; Lefrançois, R.; Buckwalter, M.R.; Nghia, N.D.; Hien, N.T.; Lortholary, O.; Poirée, S.; Manuguerra, J.C.; Gessain, A.; et al. Litchi-associated acute encephalitis in children, Northern Vietnam, 2004–2009. *Emerg. Infect. Dis.* **2012**, *18*, 1817–1824. [CrossRef] [PubMed]
16. Koul, B.; Singh, J. Lychee biology and biotechnology. In *The Lychee Biotechnology*; Springer: Berlin/Heidelberg, Germany, 2017; pp. 137–192.
17. Huang, X. Lychee production in China. In *Lychee Production in the Asia-Pacific Region*; Food and Agricultural Organization of the United Nations: Bangkok, Thailand, 2002; pp. 41–54.
18. Hai, V.M.; Dung, N.; Papaddemetriou, M.; Dent, F. Lychee production in Viet Nam. In *Lychee Production in the Asia-Pacific Region*; Food and Agriculture Organization Regional Office for Asia and the Pacific: Bangkok, Thailand, 2002; pp. 114–119.
19. Jayasinghe, S.L.; Kumar, L. Modeling the climate suitability of tea [*Camellia sinensis* (L.) O. Kuntze] in Sri Lanka in response to current and future climate change scenarios. *Agric. For. Meteorol.* **2019**, *272–273*, 102–117. [CrossRef]
20. Charoenkit, N.; Naphrom, D.; Sruamsiri, P.; Sringarm, K.; Fukuda, S. Modeling the Relationship between Hormone Dynamics and Off-season Flowering of Litchi by Using Random Forests. *Agric. Agric. Sci. Procedia* **2015**, *5*, 9–16. [CrossRef]
21. Bajpai, A.; Muthukumar, M.; Singh, A.; Nath, V.; Ravishankar, H. Narrow genetic base of Indian litchi (*Litchi chinensis*) cultivars based on molecular markers. *Indian J. Agric. Sci.* **2016**, *86*, 448–455. [CrossRef]
22. Zhao, L.; Wang, K.; Wang, K.; Zhu, J.; Hu, Z. Nutrient components, health benefits, and safety of litchi (*Litchi chinensis* Sonn.): A review. *Compr. Rev. Food Sci. Food Saf.* **2020**, *19*, 2139–2163. [CrossRef]
23. Chu, Y.-C.; Lin, T.-S.; Chang, J.-C. Pollen Effects on Fruit Set, Seed Weight, and Shriveling of '73-S-20' Litchi- with Special Reference to Artificial Induction of Parthenocarpy. *HortScience* **2015**, *50*, 369–373. [CrossRef]

24. Food and Agriculture Organization of the United Nations (FAO). *Report of the Expert Consultation on Lychee Production in the Asia-Pacific Region*; FAO: Rome, Italy, 2002. Available online: https://openknowledge.fao.org/bitstreams/efe1d554-8e16-4468-aaf1-1ce17a62d57c/download (accessed on 5 January 2025).
25. Nath, V.; Kumar, G.; Pandey, S.D.; Gupta, A.K. Status of litchi in India. *Acta Hortic.* **2018**, *1211*, 153–160. [CrossRef]
26. Kazan, K.; Lyons, R. The link between flowering time and stress tolerance. *J. Exp. Bot.* **2016**, *67*, 47–60. [CrossRef]
27. Stern, R.A.; Gazit, S. The reproductive biology of the lychee. *Hortic. Rev.* **2003**, *28*, 393–453.
28. Carr, M.K.V.; Menzel, C.M. The Water Relations and Irrigation Requirements of Lychee (*Litchi chinensis* Sonn.): A Review. *Exp. Agric.* **2014**, *50*, 481–497. [CrossRef]
29. Malhotra, S.; Singh, S.K.; Nath, V. Physiology of flowering in litchi (*Litchi chinensis*): A review. *Indian J. Agric. Sci.* **2018**, *88*, 1319–1330. [CrossRef]
30. He, P.; Liu, S.Y.; Wu, C.M.; Fu, Y.X.; Dai, P.F. Analysis of the Relationship between Lychee Yield in Qinzhou City, Guangxi and Meteorological Conditions. *Anhui Agric. Sci.* **2008**, 993–994+1164. [CrossRef]
31. Hu, F.C.; Chen, Z.; Wu, F.Z.; Fan, H.Y.; Feng, X.J.; Wang, X.H. The Current Situation and Countermeasures Suggestions of the Development of Lychee Industry in Hainan. *Chin. Trop. Agric.* **2020**, 29–33.
32. Hainan Provincial Bureau of Statistics; Survey Office of the National Bureau of Statistics in Hainan. *Hainan Statistical Yearbook 2001–2023*; China Statistics Press: Beijing, China, 2023.
33. Zhang, W.; Li, J.; Xie, Y.; He, Y. Optimization of grain yield prediction model in Henan Province based on MODIS and machine learning. *Food Sci. Technol. Econ.* **2025**, *50*, 35–40+54. [CrossRef]
34. Lai, W.Y. A Study on Sequential K-Nearest Neighbor (SKNN) Imputation for Treating Missing Rainfall Data. *Int. J. Adv. Trends Comput. Sci. Eng.* **2019**, *8*, 363–368. [CrossRef]
35. Bühlmann, P.; Yu, B. Analyzing Bagging. *Ann. Stat.* **2002**, *30*, 927–961. [CrossRef]
36. Hastie, T.; Tibshirani, R.; Friedman, J. *The Elements of Statistical Learning*; Springer Series in Statistics; Springer: New York, NY, USA, 2009; ISBN 978-0-387-84857-0.
37. Sikhandakasmita, P.; Kataoka, I.; Mochioka, R.; Beppu, K. Impact of Temperatures During Fruit Development on Fruit Growth Rate and Qualities of 'KU-PP2' Peach. *Hortic. J.* **2022**, *91*, 152–156. [CrossRef]
38. Benlloch-González, M.; Sánchez-Lucas, R.; Bejaoui, M.A.; Benlloch, M.; Fernández-Escobar, R. Global warming effects on yield and fruit maturation of olive trees growing under field conditions. *Sci. Hortic.* **2019**, *249*, 162–167. [CrossRef]
39. Feng, C.Y. The effects of covering with mulch films and reflective films on increasing the yield and quality of Wenzhou tangerines. *Zhejiang Citrus* **2002**, 18–20.
40. Zhou, L.Y.; Mo, W.P.; Zhang, J.Y.; Huang, J.B.; Bei, X.W.; Fu, X.Y.; Wang, H.C.; Huang, X.M. The Effects of Shade on the Photosynthetic Characteristics and Mineral Nutrient Accumulation of Lychee. *J. Fruit Sci.* **2014**, *31*, 270–275. [CrossRef]
41. Lai, H.X.; Li, W.G.; Peng, L.Z.; He, Y.Z.; Ling, L.L.; Chun, C.P. The effect of different colored shading nets in preventing heat-induced sunburn of navel oranges during hot days. *J. Fruit Sci.* **2022**, *39*, 1241–1251. [CrossRef]
42. Topali, C.; Antonopoulou, C.; Chatzissavvidis, C. Effect of Waterlogging on Growth and Productivity of Fruit Crops. *Horticulturae* **2024**, *10*, 623. [CrossRef]
43. Cheng, Z.H.; Kuang, Z.M.; Tao, W.; Rong, O.Z.; Ma, R.S. Multi-sugar-cane yield prediction based on random forest. *Sugarcane Ind.* **2025**, *54*, 11–18.
44. Yang, H.F.; Li, J.; Yu, S.; Wu, Y.; Liu, P.Z.; Zhang, Y. Research on Facility Cucumber Growth Model Based on Random Forest—Bayesian Optimization. *J. Shandong Agric. Univ. (Nat. Sci. Ed.)* **2024**, *55*, 314–321.
45. Chlingaryan, A.; Sukkarieh, S.; Whelan, B. Machine learning approaches for crop yield prediction and nitrogen status estimation in precision agriculture: A review. *Comput. Electron. Agric.* **2018**, *151*, 61–69. [CrossRef]
46. Hu, X.X.; Zhao, X.; Zhang, Q.; Li, Y.L.; Kong, X.S.; Ma, Y.T. Weight Analysis of Influencing Factors on Agricultural Product Yield Based on Random Forest Algorithm. *Gansu Sci. Technol.* **2020**, *36*, 16–19+40.
47. Guo, S.M.; Chen, Y.J.; Su, Y.X.; Zhong, S.Q.; Li, Z. Research on the Precise Agricultural Climate Zoning and Application of Lychees in Guangxi. *Chin. J. Agric. Sci.* **2011**, *27*, 205–209.
48. Bai, H.Q.; Wu, J.G.; Pan, X.B. Analysis of Key Climatic Factors Affecting the Distribution of Lychees in China. *J. Fruit Sci.* **2016**, *33*, 436–443. [CrossRef]
49. China News Network. Farmers Launch Self-Rescue Efforts in Fields. Available online: https://www.chinanews.com/tp/2024/09-11/10284395.shtml (accessed on 5 January 2025).
50. Zhou, W.J.; Wang, X.H.; Zhou, R.Y.; Wu, W.D.; Fan, H.Y.; Feng, X.J.; Chen, Z.; Hu, F.C. The introduction and performance of the new lychee variety "Lingfeng Rou" in Hainan. *Fruits South. China* **2023**, *52*, 85–88. [CrossRef]

51. Li, H.L.; Wang, J.B.; Zhang, L.; Zhou, J.F.; Wang, X.H.; Li, S.G.; Hu, F.C.; Sheng, Z.; Wang, G.; Wang, S.J.; et al. The introduction and performance of the extremely early-maturing lychee variety "Science No. 1" in Lingshui, Hainan. *Fruits South. China* **2024**, *53*, 70–73. [CrossRef]
52. Hu, F.C.; Zhou, W.J.; Chen, Z.; Zhou, R.Y.; Wang, M.X.; Wang, X.H. The introduction and performance of the early-maturing new variety of lychee, "Guai Zao Li", in Lingshui, Hainan Province. *Fruits South. China* **2020**, *49*, 89–93. [CrossRef]

Disclaimer/Publisher's Note: The statements, opinions and data contained in all publications are solely those of the individual author(s) and contributor(s) and not of MDPI and/or the editor(s). MDPI and/or the editor(s) disclaim responsibility for any injury to people or property resulting from any ideas, methods, instructions or products referred to in the content.